CANMET

Canada Centre for Mineral and Energy Technology

Centre canadien de la technologie des minéraux et de l'énergie

Mining Research Laboratories

Laboratoires de recherche minière

Energy, Mines and Resources Canada

Énergie, Mines et Ressources Canada

Canada

THE ENERGY OF OUR RESOURCES · THE POWER OF OUR IDEAS

L'ÉNERGIE DE NOS RESSOURCES · NOTRE FORCE CREATRICE

VISROCK

An Elasto-ViscoPlastic Program for Rocks
Theoretical Manual, version 1.0

Richard G. WAN

MRL 92-036(TR) April 1992

This document is an unedited
in-line report prepared primarily
for [illegible] and internal
[illegible] It has not
[illegible]
[illegible]
for [illegible]
(CANMET)

Ce document est un rapport
préliminaire non-révisé et rédigé
principalement pour fin de
discussion et de documentation
interne. Il ne représente nulle-
ment l'approbation définitive de
l'auteur ou Centre canadien de
la technologie des minéraux et de
l'énergie (CANMET)

MICROMEDIA

50 pp

Disclaimer: Neither the author nor the Mining Research Laboratories, Canada Centre for Mineral and Energy Technology, can accept responsibility for the correctness of the results obtained from the use of this software package.

Crown Copyright Reserved

Theoretical Manual

for

VISROCK

An Elasto-ViscoPlastic Program for Rocks

Version 1.0

©

Richard Wan, Ph. D

April 1992

92-06298/

Abstract

This report describes the theoretical background and testing of the finite element program VISROCK for the stress analysis of time dependent behaviour of mining structures. The model which is involved in this study aims at phenomenologically reproducing the main features of the creep behaviour of potash by blending the notion of viscoplastic regularization with concepts of strength degradation via cohesion and friction softening. The yield surface is based on either von Mises, Mohr-Coulomb or Drucker-Prager criterion to characterize material strength while time dependent plastic deformations follow either a simple power law or an exponential decay. The time marching scheme hinges around an implicit algorithmic framework to avoid numerical instability and secure accuracy in computations. Numerical results are presented for a complete boundary value problem which includes the analysis of a mine in Saskatchewan for illustration purposes.

Résumé

Ce rapport traite les concepts théoriques implantés dans VISROCK, logiciel d'élements finis adapté pour la modélisation du comportement différé des structures minières. L'étude a pour but de modéliser le fluage de la potasse par la théorie de la viscoplasticité. En outre, on tient compte d'une baisse de résistance de la potasse par radoucissement de la cohésion et du frottement. La résistance du matériau est représentée par des critères de rupture classiques tels que von Mises, Mohr-Coulomb, et Drucker-Prager. Par contre, les déformations plastiques différées sont décrites par une loi du type puissance ou un exponentiel. Un logiciel avec pré et post processeurs (VISROCK) a été conçu basé sur la méthode des éléments finis en bi-dimensionnel pour le calcul du champ de contrainte et déformation dans des mines de potasse profondes. L'intégration dans le temps se fait suivant une méthode implicite pour palier aux problèmes d'instabilité numérique et assurer la précision. Les calculs et résultats numériques d'une mine de potasse au Saskatchewan sont présentés à la fin de ce rapport.

Acknowledgements

The present work was funded by the Potash Corporation of Saskatchewan Inc., Technical Services and their support is gratefully acknowledged. Also the author wishes to express his sincere gratitude to the Mining Research Laboratory staffs who were involved in this project.

Contents

Abstract i

Acknowledgements ii

Nomenclature vi

1.0 Introduction 1

1.1 General Remarks 1

2.0 Objectives and Scopes 2

3.0 Theory of Elasto-viscoplasticity 3

3.1 Experimental Observations 3
3.2 Analytical Methods 3
3.3 Elasto-Viscoplastic Model 4
3.4 Assumptions 5
3.5 Governing Equations 5
3.6 Viscoplastic Algorithm 8
3.7 Time stepping 11
3.8 Cohesion and Friction Softening 11

4.0 Case Study 13

4.1 Geological Setting 13
4.2 Numerical Analysis 13
4.2.1 Finite Element Mesh 13
4.2.2 In-situ Stresses 16
4.2.3 Excavations 16
4.3 Numerical Results 18
4.3.1 Room Convergence 18
4.3.2 Stress Distribution 18
4.4 Conclusions 25

References 34

Appendix A 35

Appendix B 39

Figures

1. Notion of Elasto-viscoplasticity in Stress Space 2
2. Typical Creep Curves for Different Constant Deviatoric Stresses for Rocks 4
3 Three-component Analogical Creep Model 5
4. Drucker-Prager and von-Mises Yield Surfaces in Principal Stress Space 7
5. Mohr-Coulomb and Tresca Yield Surfaces in Principal Stress Space 7
6. Hardening/Softening Law for Simulating Tertiary Creep 12
7. Numerical Simulation of Triaxial Creep Test 12
8. Mesh Layout for Potash Mine 14
9. Details of Excavation Sequence 17
10. Comparisons of Computed Room Closures with Extensometer Readings: Pass 1 19
11. Comparisons of Computed Room Closures with Extensometer Readings: Pass 2 20
12. Comparisons of Computed Room Closures with Extensometer Readings: Pass 3 21
13. Comparisons of Computed Room Closures with Extensometer Readings: Pass 4 22
14. Evolution of Horizontal Stress in Pillar and Abutment with Mining 23
15. Evolution of Vertical Stress in Pillar and Abutment with Mining 23
16. Evolution of Viscoplastic Flow Zones with Mining Steps 24
17. Major Principal Stresses at time T = 0.007 days 26
18. Major Principal Stresses at time T = 14 days 27
19. Major Principal Stresses at time T =30 days 28

20. Major Principal Stresses at time T =48 days.....29

21. Major Principal Stresses at time T = 67 days.....30

22. Major Principal Stresses at time T =129 days.....31

23. Major Principai Stresses at time T = 244 days.....32

24. Major Principal Stresses at time T = 764 days.....33

B.1 Description of motion for excavation/fill.....42

Tables

1. Algorithm for Viscoplasticity.....10

2. Summary of Material Properties used in the Model.....15

A.1 Flow Vector Constants for Different Yield Functions.....35

A.2 Derivatives of Constants C2 for Different Yield Functions.....37

A.3 Derivatives of Constants C3 for Different Yield Functions.....38

Nomenclature

I_1, J_2 = First stress invariant and second deviatoric stress invariant

F, G, F_o = yield function, plastic potential and constant which normalizes yield function

$\mathbf{f}, \mathbf{B}^T, \mathbf{C}^E$ = external load vector, strain-displacement matrix and elastic tensor

$\mathbf{D}^T, \mathbf{K}^T$ = tangential elasto-viscoplastic and tangential stiffness matrices

$\mathbf{N}^T$ = matrix containing shape functions

$\mathbf{H}$ = Hessian matrix which contains second partial derivatives of F

$\mathbf{1}$ = Kronecker delta tensor; $\mathbf{1}_{ij} = 1$ if $i=j$, else $\mathbf{1}_{ij} = 0$

H_1, H_2 = moduli which prescribe both cohesion and friction softening

K_o = coefficient of lateral pressures at rest

M, n, c = creep function constants and cohesion

$\mathbf{s}$ = deviatoric stress tensor

trace = operator for sum of diagonal term of a matrix

det = operator for determinant of a matrix

Greek letters

α, η = time integration parameter and viscosity

$\boldsymbol{\sigma}, \dot{\boldsymbol{\sigma}}, \boldsymbol{\varepsilon}, \dot{\boldsymbol{\varepsilon}}, \dot{\boldsymbol{\varepsilon}}^e, \dot{\boldsymbol{\varepsilon}}^{vp}$ = stress, stress rate, strain, strain rate, elastic and viscoplastic strain rates tensors

θ = Lode angle (related to third stress invariant)

$\omega(t)$ = weighted time function

Ω, Γ = domain of interest and boundary

$\boldsymbol{\Phi}, \varphi, \boldsymbol{\Psi}$ = creep function, friction angle, residual load vector

$\bar{\varepsilon}^{vp}, \bar{\varepsilon}^{vp}_{cut-off}, \sigma_y$ = effective, cut-off viscoplastic strains and yield stress

$\otimes$ = tensor multiplication operator

1.0 Introduction

1.1 General Remarks

Geomaterials in general exhibit history dependent inelastic deformation resulting into non-linear behaviour. For example, the non-linearity in rocks can be attributed to the formation, closure or opening of joints within the structure. Mechanisms such as microslips, grating and remoulding which take place at the boundary of grains are responsible for the non-linear deformational behaviour observed in sands, while in clays gliding of microscopic sheets or layers is the dominant mechanism.

The phenomenon of time dependent deformations is commonly observed in underground works where the opening of excavations is the main mechanical load. For instance, the most intriguing situation occurs in rock salt caverns which continue to deform, even several months and years after excavation, to the extent of complete closure of openings. The engineer is obviously faced with the problem of adequately predicting the ultimate behaviour of the opening based only upon observations made during the excavation period. It is thus imperative to perform long range laboratory tests in order to understand the constitutive behaviour of the material and develop a model which can be used in a finite element program. Also, calibration of the model will have to be done based on field monitoring and observations.

Time dependent effects in the constitutive behaviour of the material can be described within the framework of elasticity or plasticity depending upon the degree of sophistication and accuracy required. As such, the models can be divided into two categories: viscoelasticity and viscoplasticity for reversible and irreversible deformations respectively.

The class of viscoelasticity involving linear material behaviour can be readily solved by transforming the problem into elasticity through the equivalence principle, provided that the loading and displacement conditions do not vary in time. Analytical solutions which describe the complete evolution of displacement or stress with time can then be easily obtained using Laplace transforms or other techniques, Cristescu (1989). However, when boundary conditions such as displacements, temperatures or pressures become complex, and linear viscoelastic behaviour is no longer valid, the governing equations have to be solved by means of an iterative process in the time domain and in some cases a limited time step interval must be prescribed for numerical stability reasons, see Newmark (1959).

The other class of model, i.e elasto-viscoplasticity, is characterized by material flow resulting from plastic (irreversible) deformation at a given level of stress and time. The viscous flow—triggered whenever the level of stress defined by some criterion is exceeded—may be associated or non-associated depending on the definition of a viscoplastic potential just as in classical plasticity, Mandel (1971). Thus for an elastic-viscoplastic material, it is considered at any time, a single region of response to strain in which the behaviour is purely elastic (elastic domain), or visco-elastic (visco-elastic domain). The bound of this domain at any time refers to the well-known yield surface which changes (evolution) with inelastic deformation, see Fig. 1. In the case of very deep excavations where hydrostatic compaction may take place and cause yielding, the surface has to be closed; however in most situations it is open. The comparison of elasto-viscoplasticity with elasto-plasticity completes the parallelism made in the previous section for elasticity and viscoelasticity.

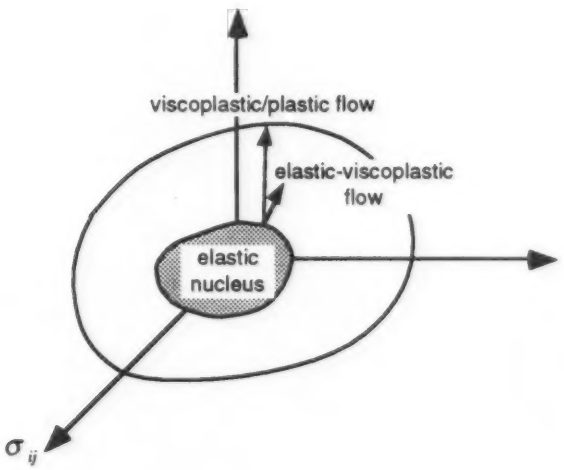

Figure 1. Notion of Elasto-viscoplasticity in Stress Space

2.0 Objectives and Scopes

The objectives of this project can be summarized as follows:

- to develop a numerical model for predicting stresses and time dependent deformations in geomaterials with an extension to potash. It will be tacitly assumed

that the behaviour of intact potash can be modelled within the framework of elasto-viscoplasticity with strain hardening and softening,

- to implement a consistent element birth/death algorithm to properly simulate backfilling and excavation activities.

3.0 Theory of Elasto-viscoplasticity

3.1 Experimental Observations

A material behaves visco-plastically if permanent deformations increase with time while loading is kept constant throughout. This so called creep behaviour can be characterized by a viscoplastic flow whose rate ideally depends on time and level of stress.

The time dependent or creep behaviour of most rocks can be subdivided into 3 fundamental parts having basic different characters namely: primary or transient creep, secondary or steady state creep and tertiary creep. Under a constant stress state, the primary creep is characterized by a strain rate decreasing with time, and is often of reversible nature, i.e. if stresses are removed, creep deformations tend to be completely recovered. However, in the secondary regime, the strain rate tends to stabilize and becomes constant with time. Usually this deformation is of irreversible nature. Experimental evidence shows that secondary creep appears when the shear stress level overcomes a given threshold and that the strain rate increases with increasing stresses. On the other hand, tertiary creep is characterized by deformation rates increasing with time and it leads to failure since strains become very large with time. Experimental data shows that the time at which tertiary creep appears, decreases with increasing shear stresses. It is also shown that dilatancy is observed for secondary and tertiary creeps for rocks. Figure 2 illustrates the typical creeping behaviours at different deviatoric stresses on a rock sample under triaxial stress conditions.

3.2 Analytical Methods

Several methods are available for the description of viscous behaviour of geomaterials. There is the generally adopted procedure which can be coined as an empirical method in which a set of laboratory tests on the material is performed under different stress conditions and a creep law derived from the experimental data. This procedure, although of practical significance, has a fundamental shortcoming. The creep law—derived from a particular set of stress and boundary conditions from curve fitting techniques—does not necessarily

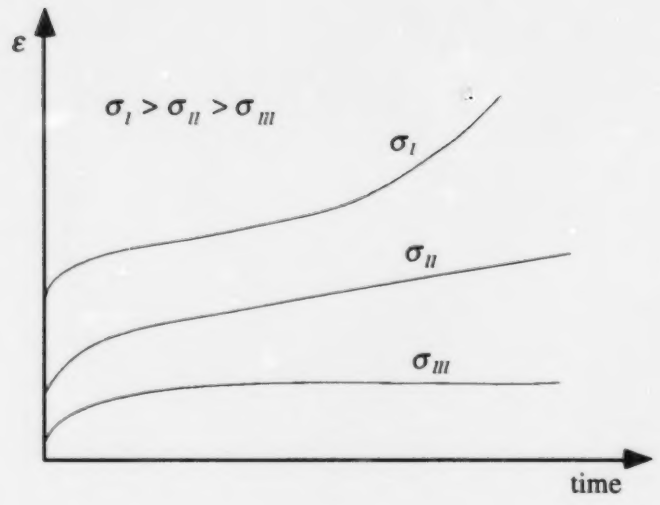

Figure 2. Typical Creep Curves for Different Constant Deviatoric Stresses for Rocks

represent the actual behaviour of the material under a general stress condition as the one met on the field. Several well-known time power laws are being widely used in practice, Carter (1985) for rock salt. Due to the empirical nature of the procedure, the derived creep law is specific to the material and stress conditions under investigation.

The other approach, more correct in nature, alludes to rheological models. The key behavioural features of the creeping material are first identified in the laboratory and then analogically represented by a system of springs, dashpots and sliders which aim at modelling the time dependent behaviour and strength characteristics of the material. In this case, only parameters related to the individual components of the rheological system need to be determined—usually by best fitting experimental data. Since the derivation is based on rheological properties of the material and not on curve fitting for a particular stress path, the law is valid for any general stress situation, without requiring additional empirical assumptions.

3.3 Elasto-Viscoplastic Model

A simple deviatoric rheological model capable of considering primary, secondary and tertiary creeps is shown in Fig. 3. The spring of modulus E accounts for elastic behaviour, while viscoplastic behaviour emanates from the slider and dashpot. Tertiary creep is modelled by assuming strength degradation with increasing viscoplastic strain rates and is herein regarded as a drop in the strength of the slider.

3.4 Assumptions

- Viscoplasticity introduces the notion of a limit stress at which and beyond which permanent deformations are not instantaneously observed but will gradually appear with time.

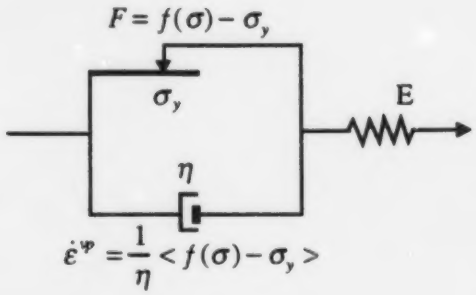

Figure 3 Three-component Analogical Creep Model

- Note that time does not come explicitly into the formulation of the constitutive law, and therefore no aging due to chemical and physical effects for example is considered. However, a constitutive law in which time effects on strength would be accounted does not have a general reach and would be specific to a given experimental observation.

- There exists in the stress space, a surface which delineates regions of elasticity and viscoplasticity. States of stresses can be found beyond that limit surface as opposed to elasto-plasticity in which the stress is restricted to remain on the yield surface.

- Only pure viscous deformations of the rock resulting from deviatoric stress states are considered. Less significant viscous deformations due to a hydrostatic stress state have been disregarded, i.e. the yield surface used is not capped.

- Tertiary creep is deemed to be due to a loss in strength (cohesion and/or friction angle) and is reflected in a drop in the threshold trigger value of the slider.

3.5 Governing Equations

In order to define the equations governing the behaviour of the rheological model, let $\dot{\sigma}$ and $\dot{\varepsilon}$ denote the stress and strain rates acting on the rheological element, Fig. 3. Depending upon the stress conditions, i.e. whether the threshold value is exceeded or not, the following situations are met:

$$F(\boldsymbol{\sigma}) < 0 \qquad \dot{\boldsymbol{\sigma}} = \mathbf{C}^{E} : \dot{\boldsymbol{\varepsilon}},$$
$$F(\boldsymbol{\sigma}) \geq 0 \qquad \dot{\boldsymbol{\varepsilon}} = \dot{\boldsymbol{\varepsilon}}^{e} + \dot{\boldsymbol{\varepsilon}}^{vp}. \tag{1}$$

The stress rate can be expressed in terms of strain rate using the elastic tensor $\mathbf{C}^{E}$,

$$\dot{\boldsymbol{\sigma}} = \mathbf{C}^{E} : (\dot{\boldsymbol{\varepsilon}} - \dot{\boldsymbol{\varepsilon}}^{vp}). \tag{2}$$

The viscoplastic strain rate is obtained by postulating a viscoplastic potential G,

$$\dot{\boldsymbol{\varepsilon}}^{vp} = \frac{1}{\eta} < \Phi\left(\frac{F}{F_0}\right) > \frac{\partial G}{\partial \boldsymbol{\sigma}}. \tag{3}$$

$G = F$ for associated flow rule and $G \neq F$ for non - associated flow rule,
η is the viscosity parameter.

<.> represents the MacCauley bracket which stands for the positive part of the argument.

The gradient to the yield/plastic potential physically represents the normal vector to the surface. In the case of an associated flow rule, the normal to the yield surface F gives the direction in which flow takes place. The function Φ is a positive monotonic regularization function which characterizes the creep law based on the yield criterion used. In general it may be a power law or an exponential represented by constants n and M, i.e.

$$\Phi\left(\frac{F}{F_0}\right) = \left(\frac{F}{F_0}\right)^{n},$$
$$\Phi\left(\frac{F}{F_0}\right) = e^{M\left(\frac{F}{F_0}\right)} - 1. \tag{4}$$

F_o is a constant used to make F non-dimensional and thus normalizes the function Φ.

The forms F used in VISROCK are based on classical yield functions such as Drucker Prager, Mohr-Coulomb, von-Mises and Tresca. An associated flow rule is adopted in this study for sake of simplicity. Figure 4 and 5 show the geometrical representation of the functions in the principal stress space.

The solution of the governing equations requires the incremental form of Eq. 3 since changes in viscoplastic strain rates must be related to increments of stresses defined by the loading history. Thus during the time interval $[t_n, t_{n+1}]$, the viscoplastic strain rates change is given by

$$d(\dot{\boldsymbol{\varepsilon}}^{vp}) = d(\frac{1}{\eta} < \Phi\left(\frac{F}{F_0}\right) > \frac{\partial G}{\partial \boldsymbol{\sigma}})$$

$$= \Gamma(< \Phi > \frac{\partial^2 G}{\partial \boldsymbol{\sigma} \otimes \partial \boldsymbol{\sigma}} + \frac{\partial < \Phi >}{\partial \boldsymbol{\sigma}} \frac{\partial G}{\partial \boldsymbol{\sigma}}) \, d\boldsymbol{\sigma},$$

in which $\Gamma = \frac{1}{\eta}$ is defined as the fluidity parameter. (5)

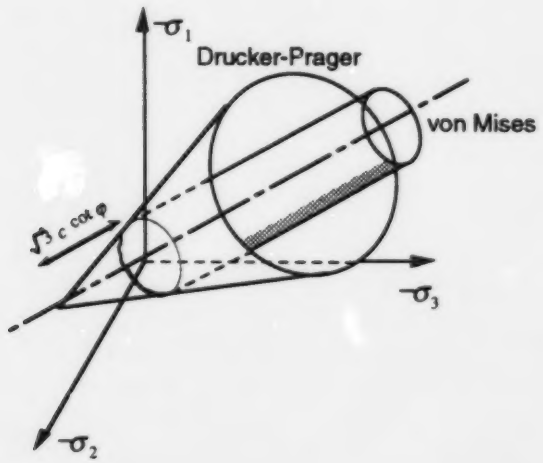

Figure 4. Drucker-Prager and von-Mises Yield Surfaces in Principal Stress Space

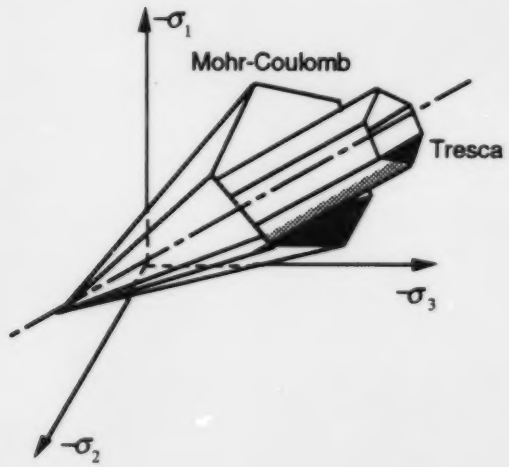

Figure 5. Mohr-Coulomb and Tresca Yield Surfaces in Principal Stress Space

Integrating over the time interval leads to the relationship between finite changes in viscoplastic strain rates and incremental stresses by means of a Hessian matrix **H** defined as

$$\Delta\dot{\boldsymbol{\varepsilon}}^{vp} = \mathbf{H} : \Delta\boldsymbol{\sigma}, \tag{6}$$

where

$$\mathbf{H} = \int_{t_n}^{t_{n+1}} \Gamma(<\Phi> \frac{\partial^2 G}{\partial\boldsymbol{\sigma} \otimes \partial\boldsymbol{\sigma}} + \frac{\partial <\Phi>}{\partial\boldsymbol{\sigma}} \frac{\partial G}{\partial\boldsymbol{\sigma}}) \, \dot{\boldsymbol{\sigma}} \, dt \tag{7}$$

and

$$\Delta\boldsymbol{\sigma} = \mathbf{C}^{E} : (\Delta\boldsymbol{\varepsilon} - \Delta\boldsymbol{\varepsilon}^{vp}). \tag{8}$$

It is noted that the calculation of the Hessian matrix involves the computation of second derivatives of the yield or plastic potential with respect to stresses. Explicit expressions of **H** for different forms of F are given in appendix A.

3.6 Viscoplastic Algorithm

The governing equations will be solved incrementally, i.e at each time step, the changes in displacements, strains, stresses and loads are computed and added at the end of the time step. The equilibrium correction emanating from viscoplastic strain rates is added to the external load vector and applied to the next time step. In this sense, the method used is very similar to the initial strain technique used in the displacement type finite element method.

The equilibrium equations as obtained from the Principle of Virtual Work during time interval $[t_n, t_{n+1}]$ is given by

$$\int_{\Omega} \mathbf{B}^{T} : \Delta\boldsymbol{\sigma}_n \, d\Omega = \Delta\mathbf{f}_n + \boldsymbol{\Psi}. \tag{9}$$

The compatibility matrix **B** relates displacements **u** to strains **ε**. It is noted that the external forces **f** need not be in exact equilibrium with internal forces and the offset is represented by the residual vector **Ψ**.

The integration of viscoplastic strain rates in the time interval $[t_n, t_{n+1}]$ can be numerically performed by using the discretized form of Eq. 6, i.e.

$$\Delta\boldsymbol{\varepsilon}_n^{vp} = \Delta t_n [(1-\alpha)\dot{\boldsymbol{\varepsilon}}_n^{vp} + \alpha \, \dot{\boldsymbol{\varepsilon}}_{n+1}^{vp}], \quad \alpha \in [0,1]. \tag{10}$$

The parameter α controls the nature of the approximation; α =0 corresponds to an explicit scheme while α =1 refers to a fully implicit scheme. Since

$$\dot{\boldsymbol{\varepsilon}}_{n+1}^{vp} = \dot{\boldsymbol{\varepsilon}}_{n}^{vp} + \Delta\dot{\boldsymbol{\varepsilon}}_{n}^{vp}, \tag{11}$$

the viscoplastic strain rate at the end of the time step can be expressed solely by values known at the beginning of the time step,

$$\Delta\boldsymbol{\varepsilon}_{n}^{vp} = \Delta t_n(\dot{\boldsymbol{\varepsilon}}_{n}^{vp} + \alpha\,\Delta\dot{\boldsymbol{\varepsilon}}_{n}^{vp}). \tag{12}$$

Substituting Eq. 6 into the above flow equation, one gets

$$\Delta\boldsymbol{\varepsilon}_{n}^{vp} = \Delta t_n(\dot{\boldsymbol{\varepsilon}}_{n}^{vp} + \alpha\,\mathbf{H}_n:\Delta\boldsymbol{\sigma}_n). \tag{13}$$

Making note of this, the stress-strain relationship represented in Eq. 8 thus becomes

$$\Delta\boldsymbol{\sigma}_n = \mathbf{C}^{\mathrm{E}}:(\Delta\boldsymbol{\varepsilon}_n - \Delta t_n\dot{\boldsymbol{\varepsilon}}_{n}^{vp} - \Delta t_n\,\alpha\,\mathbf{H}_n:\Delta\boldsymbol{\sigma}_n). \tag{14}$$

Finally rearranging terms gives

$$\Delta\boldsymbol{\sigma}_n = \mathbf{D}_n^{T}:(\Delta\boldsymbol{\varepsilon}_{n}^{vp} - \Delta t_n\dot{\boldsymbol{\varepsilon}}_{n}^{vp}), \tag{15}$$

where

$$\mathbf{D}_n^{T} = (\mathbf{C}^{\mathrm{E}^{-1}} + \alpha\Delta t_n\mathbf{H}_n)^{-1}. \tag{16}$$

When the stress increment relationship in Eq. 14 is substituted into Eq. (9), the finite element equilibrium equation becomes

$$\mathbf{K}^{T}\Delta\mathbf{u}_n - \Delta\mathbf{f}_{n}^{vp} - \Delta\mathbf{f}_n = \boldsymbol{\Psi}_n, \tag{17}$$

in which the tangential stiffness is given as

$$\mathbf{K}^{T} = \int_{\Omega}\mathbf{B}^{\mathrm{T}}:\mathbf{D}_n^{T}:\mathbf{B}\,d\Omega, \tag{18}$$

and the correction nodal forces due to viscoplastic deformations are

$$\Delta\mathbf{f}_{n}^{vp} = \Delta t_n\int_{\Omega}\mathbf{B}^{\mathrm{T}}:\mathbf{D}_n^{T}:\dot{\boldsymbol{\varepsilon}}_{n}^{vp}\,d\Omega. \tag{19}$$

The schematic procedure for the finite element solution including excavation/fill is summarized in Table 1.

Table 1. Algorithm for Viscoplasticity;

Let $[t_n, t_{n+1}] \in R^+$ be a typical time of interest

1. Data base at t_n: $\{\mathbf{u}_n, \boldsymbol{\varepsilon}_n, \boldsymbol{\sigma}_n, \boldsymbol{\varepsilon}^{vp}_n, \dot{\boldsymbol{\varepsilon}}^{vp}_n, \mathbf{f}_n\}$
   IF $n = 0$ THEN

2. • Elastic run
   $\dot{\boldsymbol{\varepsilon}}^{vp}_n \equiv 0; \quad \Delta\mathbf{f}^{vp}_0 \equiv 0; \quad \mathbf{D}^T_0 \equiv \mathbf{C}^E; \quad \boldsymbol{\Psi}_n \equiv 0; \quad \mathbf{K}^T_n = \int_\Omega \mathbf{B}^T : \mathbf{C}^E : \mathbf{B}\, d\Omega$

   ELSE

3. • Elasto - Visco - Plastic run
   IF $\tau \in [t_n, t_{n+1}] \subset \Im$:{set of excavation / fill times}
   Define set of active elements

   FOR ALL ACTIVE ELEMENTS
   • Form tangential modulus $\mathbf{D}^T_n$

   $$\mathbf{D}^T_n = \left[\mathbf{C}^{E^{-1}} + \mathbf{C}_n\right]^{-1}$$

   $\mathbf{C}_n = \alpha \Delta t_n \mathbf{H}_n$ $\mathbf{H}_n$: Hessian Matrix
   and hence tangential stiffness $\mathbf{K}^T_n$

   $$\mathbf{K}^T_n = \int_\Omega \mathbf{B}^T : \mathbf{D}^T_n : \mathbf{B}\, d\Omega$$

   • Form residual load vector and pseudo - loads due to viscoplastic strain rates

   $$\boldsymbol{\Psi}_n = \mathbf{f}_n + \Delta\mathbf{f}_n - \int_\Omega \mathbf{B}^T : \boldsymbol{\sigma}_n\, d\Omega$$

   NEXT ELEMENT
   ENDIF

4. Solve system of linearized equations:
   $\mathbf{K}^T_n . \Delta\mathbf{u}_n = \Delta\mathbf{f}^{vp}_n + \boldsymbol{\Psi}_n \quad ; \Delta\mathbf{f}^{vp}_n = \Delta t_n \int_\Omega \mathbf{B}^T : \mathbf{D}^T : \dot{\boldsymbol{\varepsilon}}^{vp}_n\, d\Omega$

5. Advance solution to t_{n+1} by incrementing all principal variables
   $\mathbf{u}_{n+1} = \mathbf{u}_n + \Delta\mathbf{u}_n, \Delta\boldsymbol{\varepsilon}_n = \mathbf{B} : \Delta\mathbf{u}_n, \boldsymbol{\varepsilon}_{n+1} = \boldsymbol{\varepsilon}_n + \Delta\boldsymbol{\varepsilon}_n$
   $\Delta\boldsymbol{\varepsilon}^{vp}_n = \Delta t_n [(1-\alpha)\dot{\boldsymbol{\varepsilon}}^{vp}_n + \alpha\, \dot{\boldsymbol{\varepsilon}}^{vp}_{n+1}], \alpha \in [0,1]$

   $$\dot{\boldsymbol{\varepsilon}}^{vp}_n = \Gamma\langle\Phi(F)\rangle \frac{\partial F}{\partial \boldsymbol{\sigma}} = \boldsymbol{\Omega} : \boldsymbol{\sigma}_n, \Delta\dot{\boldsymbol{\varepsilon}}^{vp}_n = \mathbf{H}_n : \Delta\boldsymbol{\sigma}_n, \dot{\boldsymbol{\varepsilon}}^{vp}_{n+1} = \dot{\boldsymbol{\varepsilon}}^{vp}_n + \Delta\dot{\boldsymbol{\varepsilon}}^{vp}_n$$

   $\Delta\boldsymbol{\sigma}_n = \mathbf{C}^e : (\Delta\boldsymbol{\varepsilon}_n - \Delta\boldsymbol{\varepsilon}^{vp}_n) = \mathbf{D}^T_n : (\Delta\boldsymbol{\varepsilon}_n - \Delta t_n\, \dot{\boldsymbol{\varepsilon}}^{vp}_n), \boldsymbol{\sigma}_{n+1} = \boldsymbol{\sigma}_n + \Delta\boldsymbol{\sigma}_n$
   $\boldsymbol{\varepsilon}^{vp}_{n+1} = \boldsymbol{\varepsilon}^{vp}_n + \Delta\boldsymbol{\varepsilon}^{vp}_n, \Delta\dot{\boldsymbol{\varepsilon}}^{vp}_n = \Delta t_n \dot{\boldsymbol{\varepsilon}}^{vp}_n$

   Determine next time step length Δt_{n+1} based on empirical criteria such as:

   $$\text{(i) } \Delta t_{n+1} \le k\, \Delta t_n; \text{ (ii)} \Delta t_{n+1} \le \tau^* \left\{ \frac{\bar{\varepsilon}_{n+1}}{\dot{\bar{\varepsilon}}^{vp}_{n+1}} \right\}_{min}$$

6. Check viscoplastic strain rates:
   IF $\dot{\boldsymbol{\varepsilon}}^{vp}_{n+1} << 0$ THEN
   Steady State has been reached: EXIT and go to next excavation / fill step
   ELSE
   $n \leftarrow: n+1$
   go to step 3
   ENDIF

3.7 Time Stepping

The rock mass viscoplastic strain rate $\dot{\varepsilon}^{vp}$ depends on two parameters, namely the fluidity parameter Γ and the time step Δt adopted in the discretization. The time step size can significantly influence the numerical results: if too large it can provoke numerical oscillations which may lead to incorrect or divergent solutions, and if too small it may mean unnecessary calculations and hence high computational costs. For explicit time stepping scheme (α=0), the integration scheme is conditionally stable and the time step must be less than a critical value derived under specific conditions by Cormeau (1975). For a more general stress situation, there is no theoretical formulation in determining that critical value, hence two empirical criteria suggested in Owen and Hinton (1980) will be used. They are found to be very useful and reasonable for practical purposes.

The first one keeps the time step interval below the minimum of the ratio of the total strains to the effective viscoplastic strain rate taken over all gauss integration points by a factorτ , i.e

$$\Delta t_{n+1} \leq \tau \left(\frac{\bar{\varepsilon}_{n+1}}{\bar{\varepsilon}^{vp}_{n+1}} \right)_{\min} \tag{20}$$

The factor τ is an empirical input parameter and for an implicit time stepping scheme, it is suggested to be in the range $0.01 < \tau < 0.15$ to obtain accurate results. The second empirical criterion simply limits the time interval change for any two consecutive intervals by using a specified constant k taken to be 1.5 in general,

$$\Delta t_{n+1} \leq k \Delta t_n \tag{21}$$

3.8 Cohesion and Friction Softening

The tertiary creep regime can be attributed to a loss of cohesion and/or friction of the material, see Fig. 6. In this study, the yield stress value F is made function of effective viscoplastic strains, a measure of viscoplastic strain history, through a simple bi-linear relationship:

$$F = F_o + (H_1 - H_2)\bar{\varepsilon}^{vp}_{cut-off} + H_2 \bar{\varepsilon}^{vp}, \tag{22}$$

where H_1 and H_2 are moduli which prescribe the desired hardening (positive value) or softening (negative value) effect, and effective viscoplastic strain is given by where H_1 and

H_2 are moduli which prescribe the desired hardening (positive value) or softening (negative value) effect, and effective viscoplastic strain is given by $\bar{\varepsilon}^{vp} = \sqrt{\frac{2}{3}\boldsymbol{\varepsilon}^{vp} : \boldsymbol{\varepsilon}^{vp}}$.

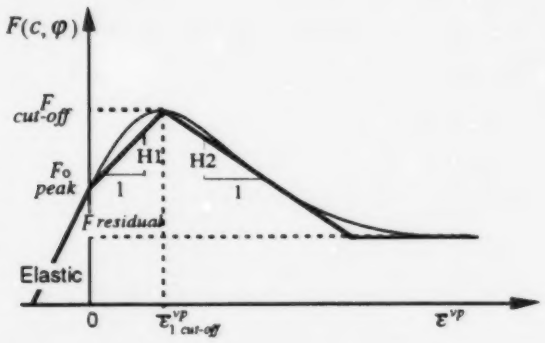

Figure 6. Hardening/Softening Law for Simulating Tertiary Creep;

The effect of friction softening is demonstrated in the numerical example shown in Fig. 7 which involves the simulation of a triaxial creep test. In this example, as viscoplastic strains become prominent at an axial stress of 90 KPa, softening takes place and tertiary creep is appropriately captured. Note that the confining pressure σ_3 is kept constant at 10 KPa throughtout the test.

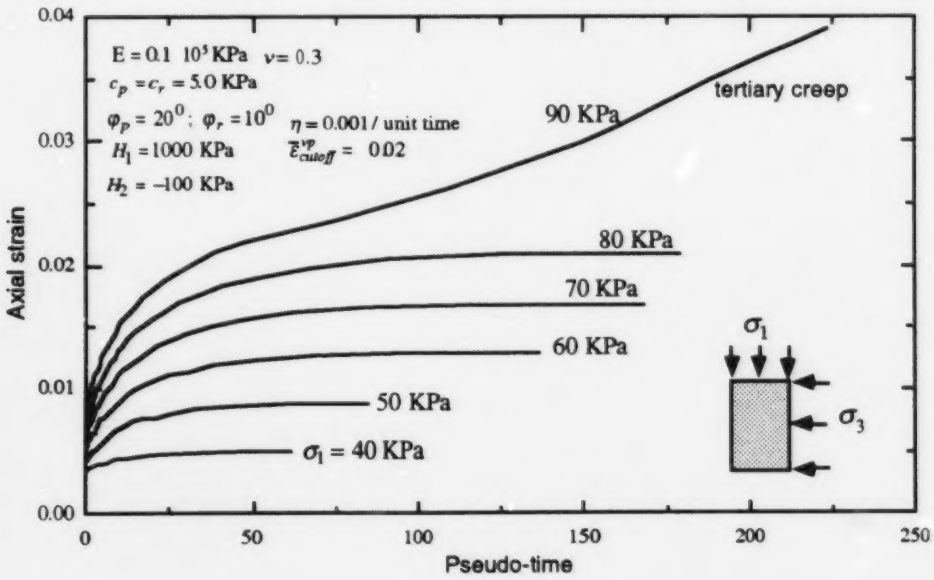

Figure7. Numerical Simulation of Triaxial Creep Test;

4.0 Case Study

The numerical example analyzed in this section of the report is related to a potash mine located in the south eastern part of Saskatchewan.

4.1 Geological Setting

South Saskatchewan is underlain by the middle Devonian potash beds where most of the mining development takes place. The mining potash layer, about 3 metres thick, is typically found at a depth of 1000 metres below ground surface and rests on the Prairie evaporites which consist of alternate beds of fairly competent halites and sylvites. Above the potash layer is a 25 metre thick upper halite formation of lower strength since it contains a thin weak clay seam. The rest of the strata is made up of the overburden containing two major formations: Second Red Bed a relatively weak geological unit and Dawson Bay a much stronger unit. The Red Bed formation consists of fairly weak dolomite mudstones while the Dawson Bay formation is a sequence of competent carbonates, bitumen and anhydride. Finally near surface, the upper most member of the Dawson Bay formation is the Hubbard evaporite which is a halite bed of variable thickness.

4.2 Numerical Analysis

4.2.1 Finite Element Mesh

The finite element mesh used in the analysis consists of 832 linear iso-parametric elements and 891 nodes, see Fig. 8. Plane strain conditions are considered and no axis of symmetry has been taken for the representation of the domain due to the nature of excavation sequence. The section shown in Fig. 8 represents a panel of two rooms located at a depth of about 960 m in the Prairie evaporite formation.

Six geological units have been used to idealize the prevalent geological conditions described in the previous section. These units, starting from the deepest, are namely: Lower Halite, Potash, Upper Halite, Clay Seam, Upper Halite, Second Red Bed Formation and Dawson Bay Formation. The geomechanical properties used to describe each material have been either taken from the existing literature, Sepehr et. al. (1988), or based on engineering judgement when information was not available. A summary of the pertinent parameters is given in Table 2. The lower halite, upper halite and potash are considered elasto-viscoplastic with constant strength once permanent deformations are triggered, i.e there is no hardening or softening effect. However for the remaining materials, loss of strength

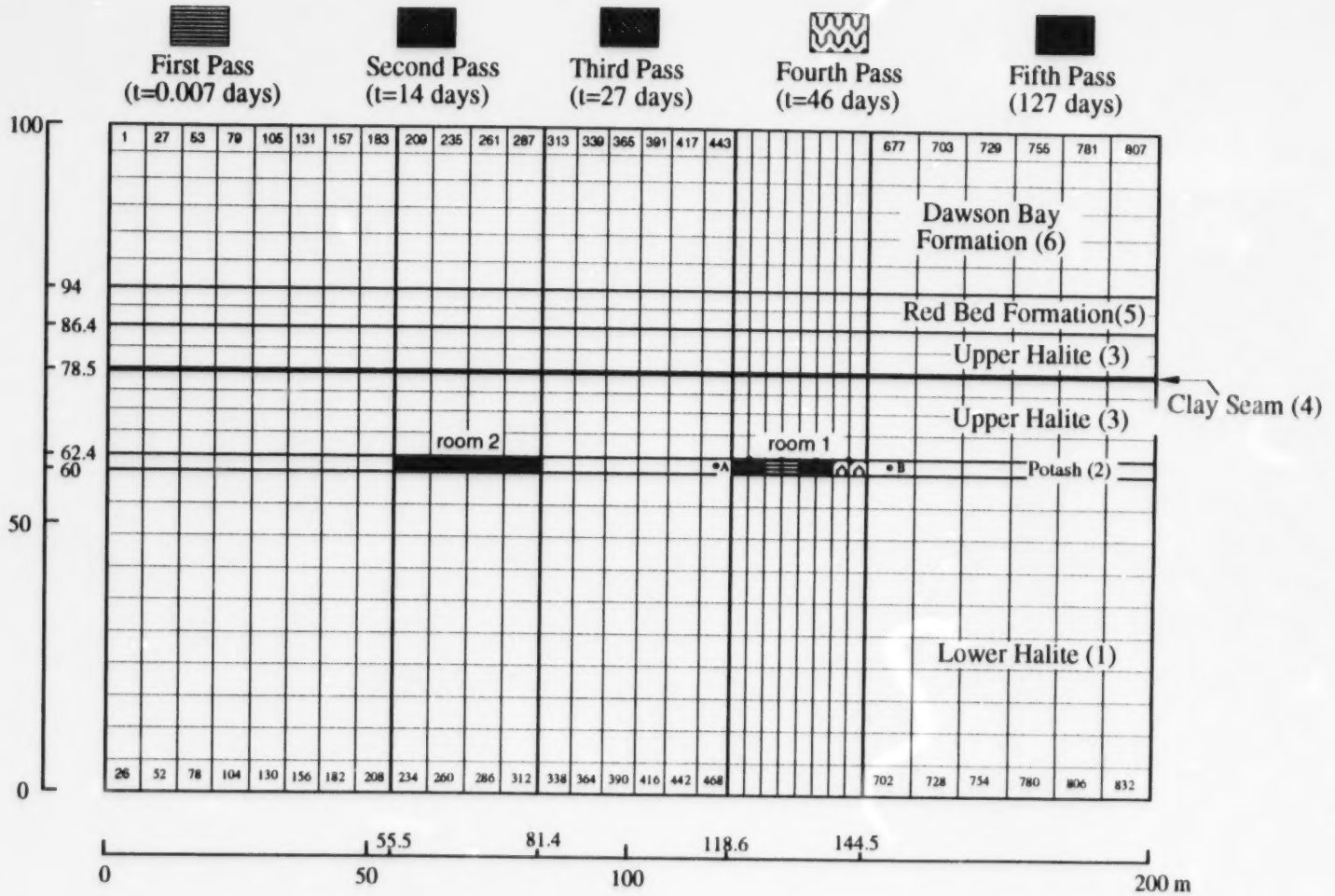

Figure 8. Mesh Layout for Potash Mine

Table 2. Summary of Material Properties used in the Model

Material Property	Halite Floor (1)	Potash (2)	Halite Roof (3)	Clay Seam (4)	Red Bed Formation (5)	Dawson Formation (6)
Young's modulus (MPa), E	5336	3268	5060	1455	14546	33011
Poisson's ratio, υ	0.46	0.46	0.46	0.44	0.27	0.28
Density (MN/m^3)	0.022	0.027	0.022	0.022	0.023	0.027
Cohesion (MPa) c	0.1	0.1	0.1 0.01(res)	10(peak) 0.01(res)	0.1(peak) 10(res)	23(peak)
Friction angle (deg) φ	28	22	25 7(res)	12(peak) 30(res)	38(peak)	46
Hardening modulus H_1 (MPa)	0	0	0	-1000	600	46667
Hardening modulus H_2 (MPa)	0	0	0	-1000	-100	-2600
Effective strain cut-off	—	—	—	0.05	0.05	0.05
Fluidity (/days), $1/\eta$	0.5 E-7	0.35E-7	0.35E-7	0.5E-7	0.5E-7	0.5E-7
Exponent number, n	4.3	4.5	4.5	4.3	4.3	4.3

is taken into account by assigning peak and residual values to cohesion and friction angles, and a softening modulus is used to describe the transition from peak to residual. Special attention is paid to the clay seam in the analysis by using a thin weak element to simulate the interface behaviour.

4.2.2 In-situ Stresses

The in-situ stress conditions prior to any excavation are simulated by "switching" or "turning" on gravity together with the application of a uniform pressure of 21.6 MPa. on the top boundary of the finite element mesh in a first step. In this case, the stress calculations depend on the in-situ unit weight, Poisson ratio used for each formation and the overburden pressure. The in-situ stress ratio K_o varies linearly from 0.39 at the top of the mesh to 0.85 at the bottom.

4.2.3 Excavations

The potash seam is mined using a long room and pillar mining system which gives an average panel recovery of 40%, while overall mine recovery is around 35%. The rooms to be excavated are 25.9 m wide separated by a 37.2 m wide pillar. The room is typically excavated in four passes each the size of the blade of the excavator. Room 1, as shown in Fig. 9, is mined out in four such passes at times 0.007, 14, 27 and 46 days respectively, while Room 2 is excavated in one pass after 127 days. The excavation sequence is simulated as closely as possible in the model since the main goal of this study is to follow the progress of mining and resulting stresses and deformations with time.

It is noted that excavation, herein, is simulated in a consistent manner and does not involve the substitution of existing elements by "air" or "void" elements, a technique frequently used by other investigators. Instead, in this study, the excavated elements are numerically removed by subtracting, in a consistent way, element stiffnesses and forces from the global array. This ensures consistency in the numerical calculations and avoids numerical instability associated to the previously mentioned technique. Appendix B gives details of the excavation/fill formulation from a finite element stand-point.

Figure 9. Details of Excavation Sequence

4.3 Numerical Results

4.3.1 Room Convergence

The room convergence measurements at each stage of the excavation has been monitored on the field and extensometers readings are readily available for points located at the centre of each pass during the mining sequence. These reading points are shown in Fig. 9. The numerical results for room closure during the progress of mining are compared with measurement for each extensometer point, see Figs. 10, 11, 12, and 13. Also, the numerical results, Yu et. al. (1987), obtained from a viscoelastic program based on an empiral power law are plotted on the same graphs for comparison. Notice the occurrence of jumps in the computed convergence curves which correspond to the beginning of each mining step. It is seen that on the whole, numerical results compare favourably well with field measurements, especially the evolutive trend is correctly captured. However, the viscoelastic results tend to give a steadily increasing closure with time while the closure rate computed from viscoplasticity eventually becomes more or less stationary with time.

In general, it is seen that computed values for convergence are systematically higher than those measured. A possible explanation for this discrepancy is that some creep may have already taken place before the extensometer was installed on the field. The convergence is maximum for the measurement point located in the first pass and is of the order of 30 cm at the end of 750 days. Less movement (15 cm) takes place at the measuring point made in the fourth pass due to the stress redistribution and deformation already taken place in the previous passes. The close match of numerical convergence values and trend support the view that the overall accuracy of the geomechanical parameters used in this study are sufficient for practical needs.

4.3.2 Stress Distribution

The evolution of stresses in the formation indicates how stresses are being redistributed as excavations proceed, and provides useful information for the determination of zones of overstress, tension or relaxation.

Figures 14 and 15 show the evolution of horizontal and vertical stresses at points selected in the abutment (B) and central pillar (A), see Fig. 9 for details. It is seen that at the beginning of each mining step, stresses in general increase due to excavation and as potash creeps, the stress level drops at a rate prescribed by its viscous property. The horizontal

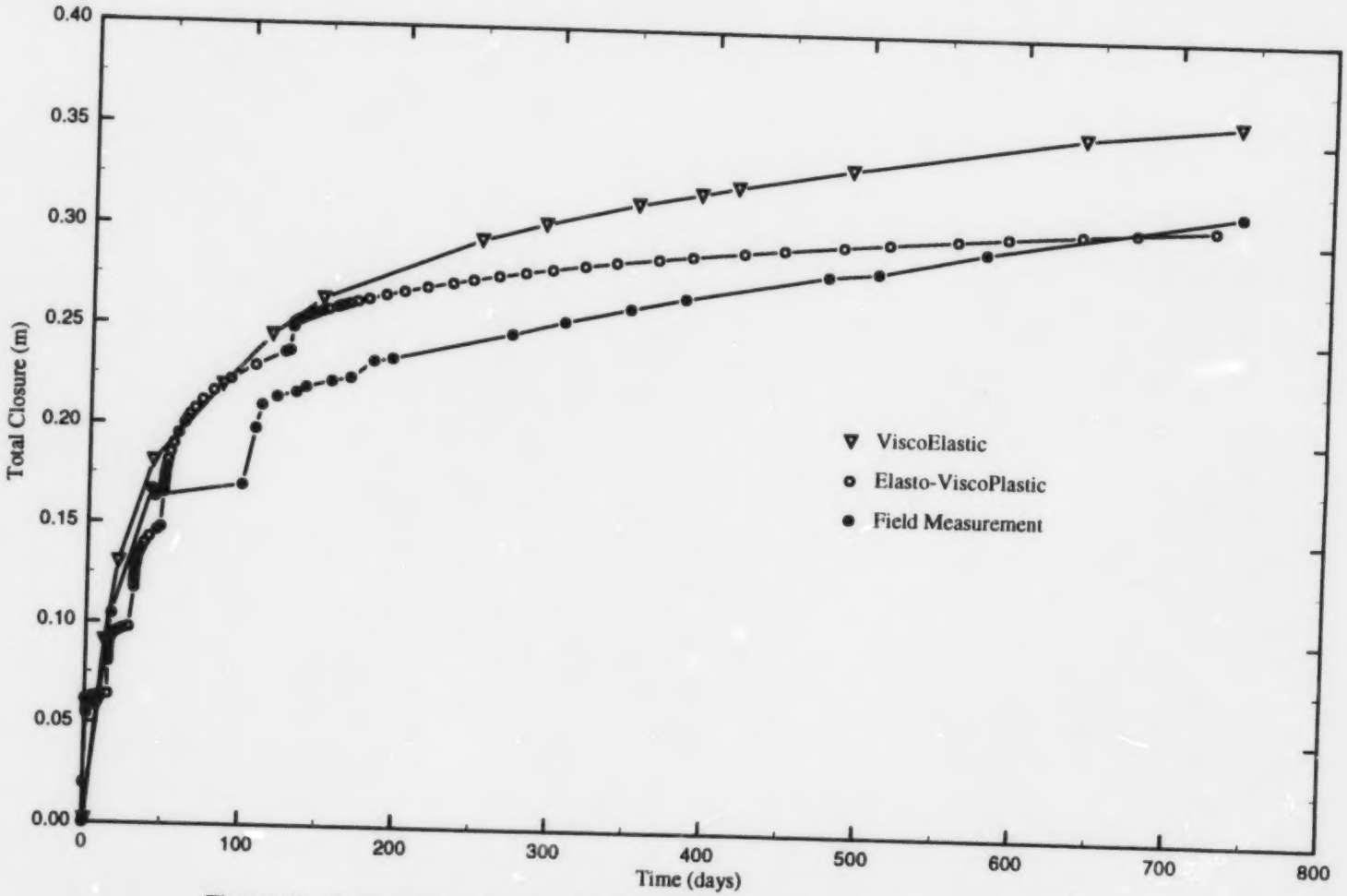

Figure 10. Comparisons of Computed Room Closures with Extensometer Readings: Pass 1

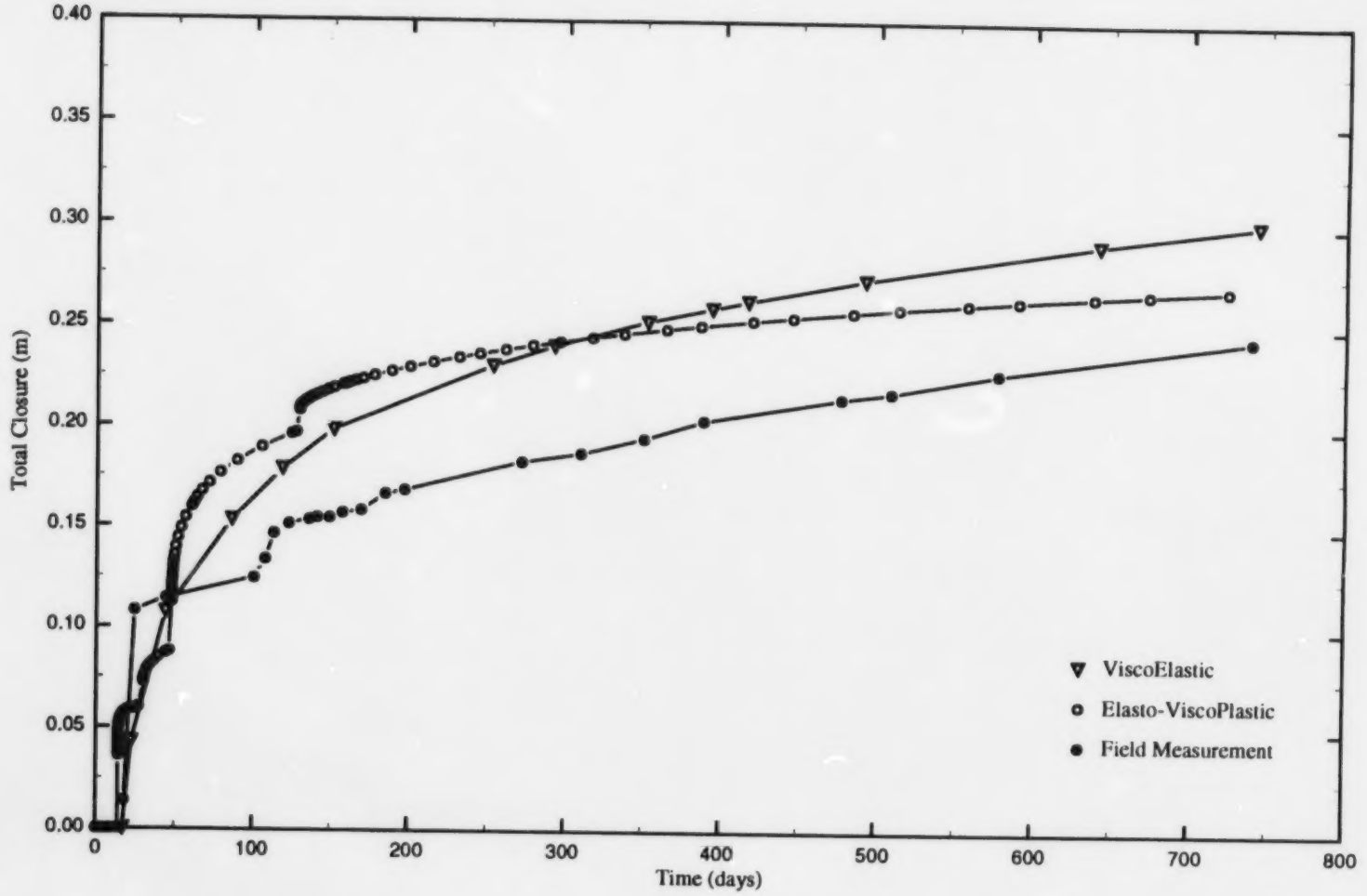

Figure 11. Comparisons of Computed Room Closures with Extensometer Readings: Pass 2

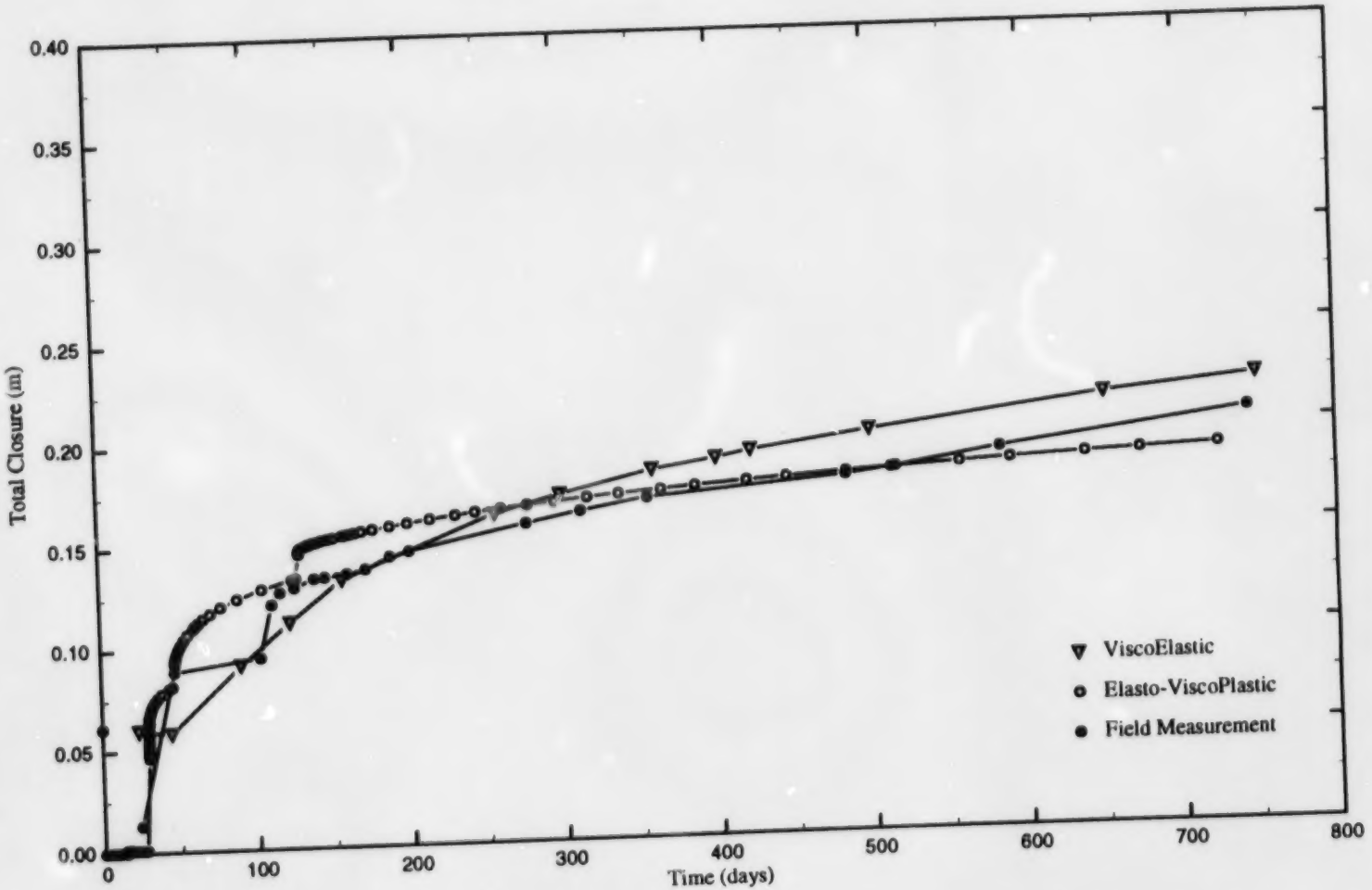

Figure 12. Comparisons of Computed Room Closures with Extensometer Readings: Pass 3

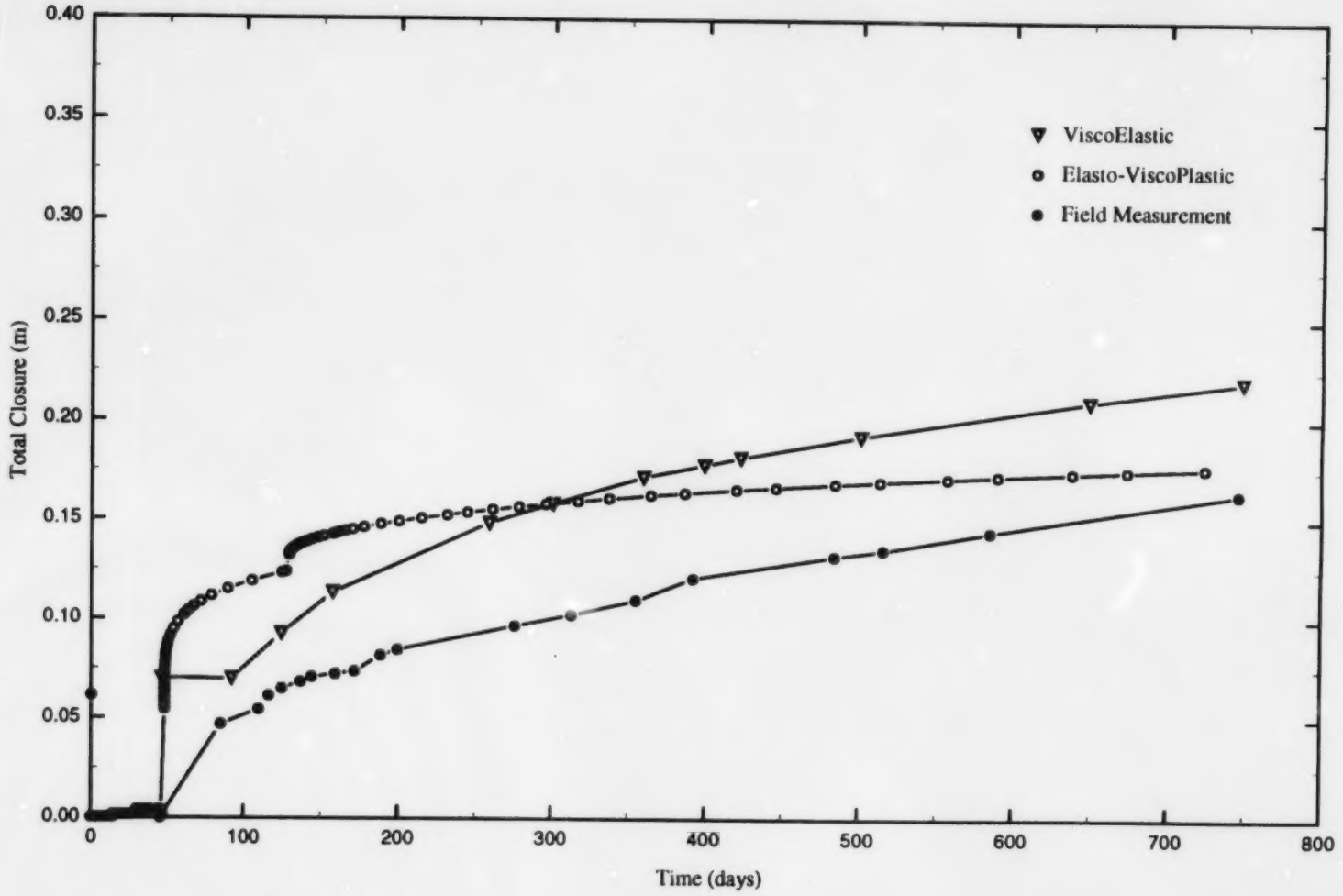

Figure 13. Comparisons of Computed Room Closures with Extensometer Readings: Pass 4

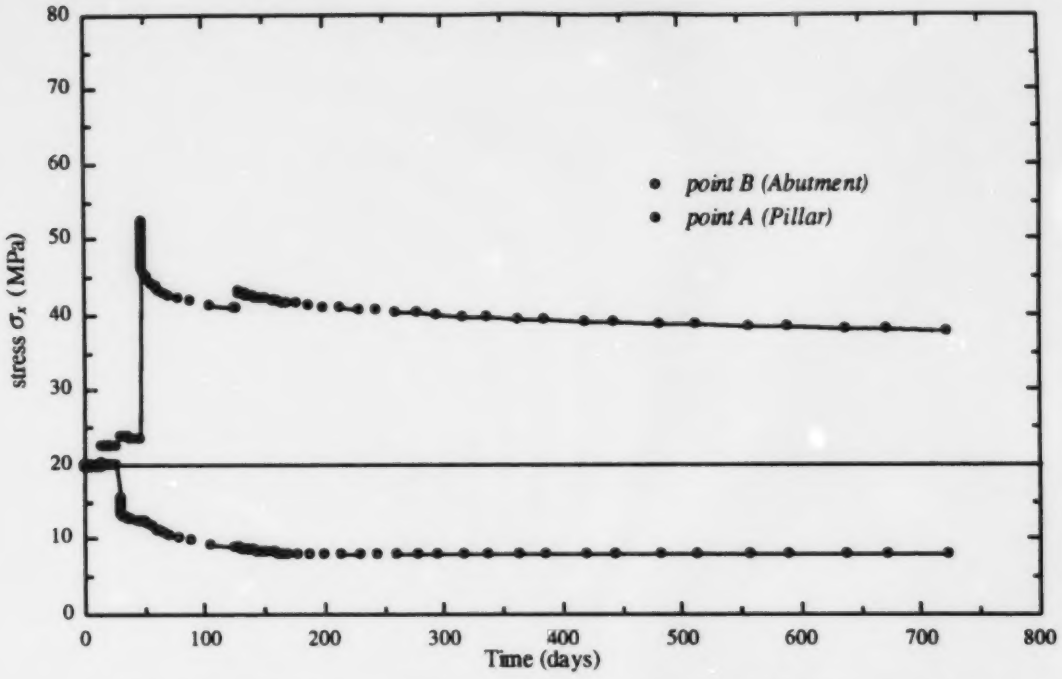

Figure 14. Evolution of Horizontal Stress in Pillar and Abutment with Mining

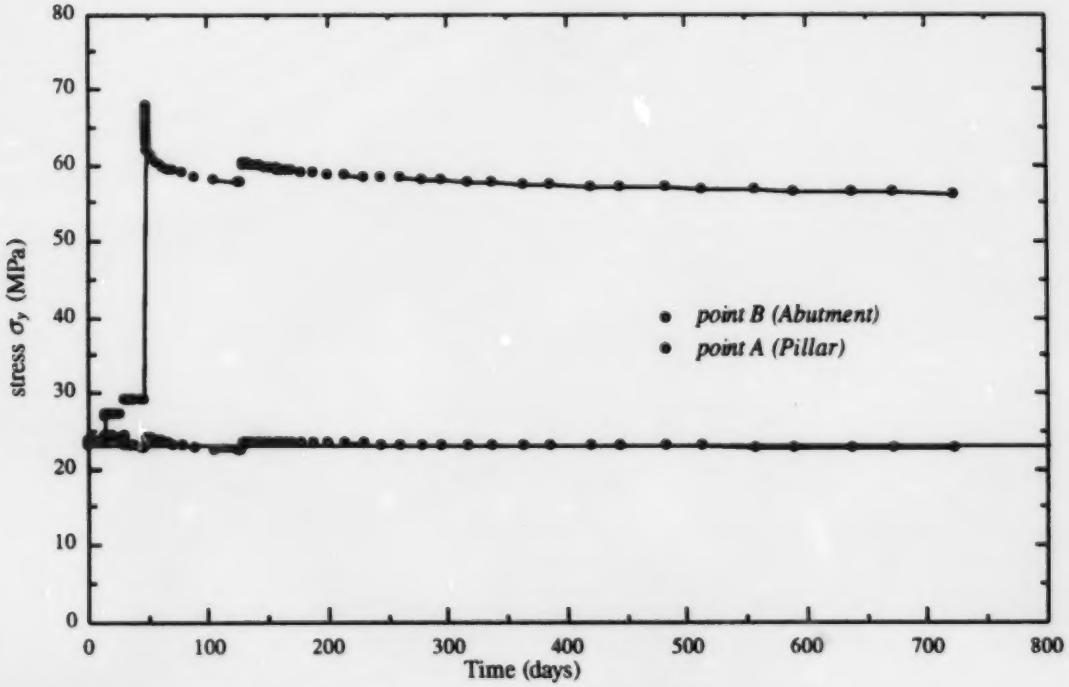

Figure 15. Evolution of Vertical Stress in Pillar and Abutment with Mining

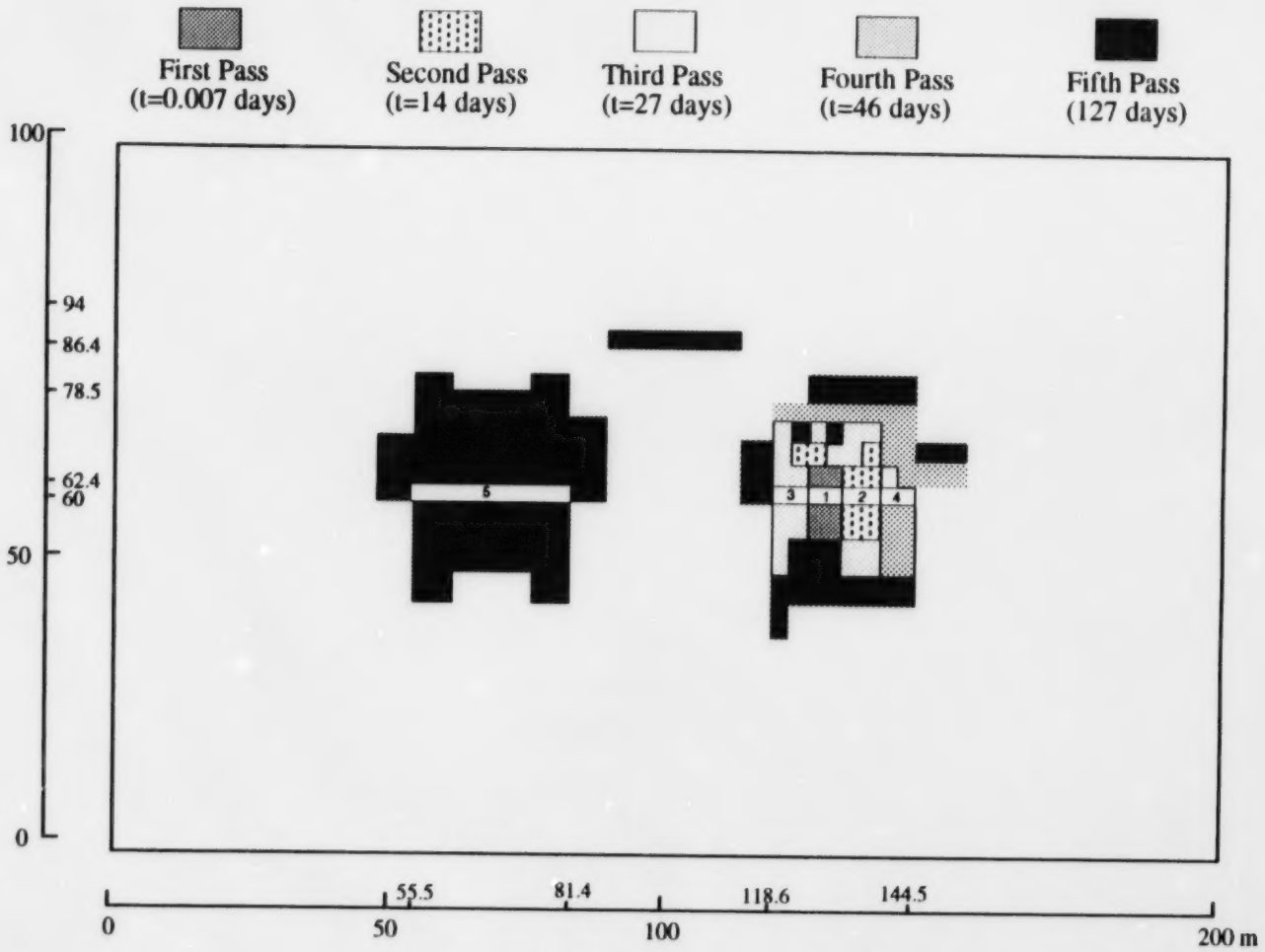

Figure 16. Evolution of Viscoplastic Flow Zones with Mining Steps

stresses in the pillar after excavation are higher than the in-situ values due to the sequence of excavation which has a bias towards point A, and thus promotes the occurrence of high stresses. The horizontal stress at point B is below in-situ level as a result of a relaxation phenomenon. The same trend is obtained for vertical stresses, see Fig. 15. It is expected that the pillar will be more susceptible to yielding than will be, the abutment. This point of view is confirmed in Fig. 16 which shows the spreading of viscoplastic or creep zones with time around the excavations, particularly in the pillar zone.

The major principal stress contours have been plotted for selected time steps to study stress redistribution due to creep as mining progresses. When the first pass is excavated after 0.007 days, overstressing of the order of 50 MPa occurs at the sidewalls, while pockets of stresses as high as 25 MPa develop at the roof and floor of the opening, see Fig. 17. Cutting of the second pass further creates overstressing around the opening, particularly at the sidewalls, as shown in Fig. 18. Furthermore, some stress relaxation as low as 10 MPa start to develop at the mid section of the roof and floor due to softening. In Figs. 19 and 20, as the two other passes are excavated, overstressing becomes more extensive as it further pervades throughout the vicinity of the opening. Also, the relaxation region in the middle section becomes more prominent, suggesting the development of considerable creeping strain activity. A well defined region of locked-up stresses below in-situ values form about 15 m above the roof. After 67 days with room 1 opened alone, the overstresses around the opening continue to permeate further away and the soft zone at the roof expands, Fig 21. When room 2 is next opened in one pass, the overstress zones around the two openings coalesce while the stress level in the abutment is releived as shown in Fig. 22. Figures 23 and 24 show the final evolution of the overstress for the rest of the time.

4.4 Conclusions

The time dependent behaviour of potash has been idealized within the framework of the theory of elasto-viscoplasticity. It is seen that the introduction of a softening phenomenon via a drop in cohesion or friction with increasing creeping strains can effectively replicate tertiary creep. A comparison of viscoelastic and elasto-viscoplastic computations with field measurements for a potash mine in Saskatchewan was done. Favourable agreement was obtained for the stress range and loading times considered. The agreement was closer than that provided by a simple viscoelastic model. The favourable finite element computations afforded in this case study suggests that VISROCK has a potential for practical applications in the potash mining industry.

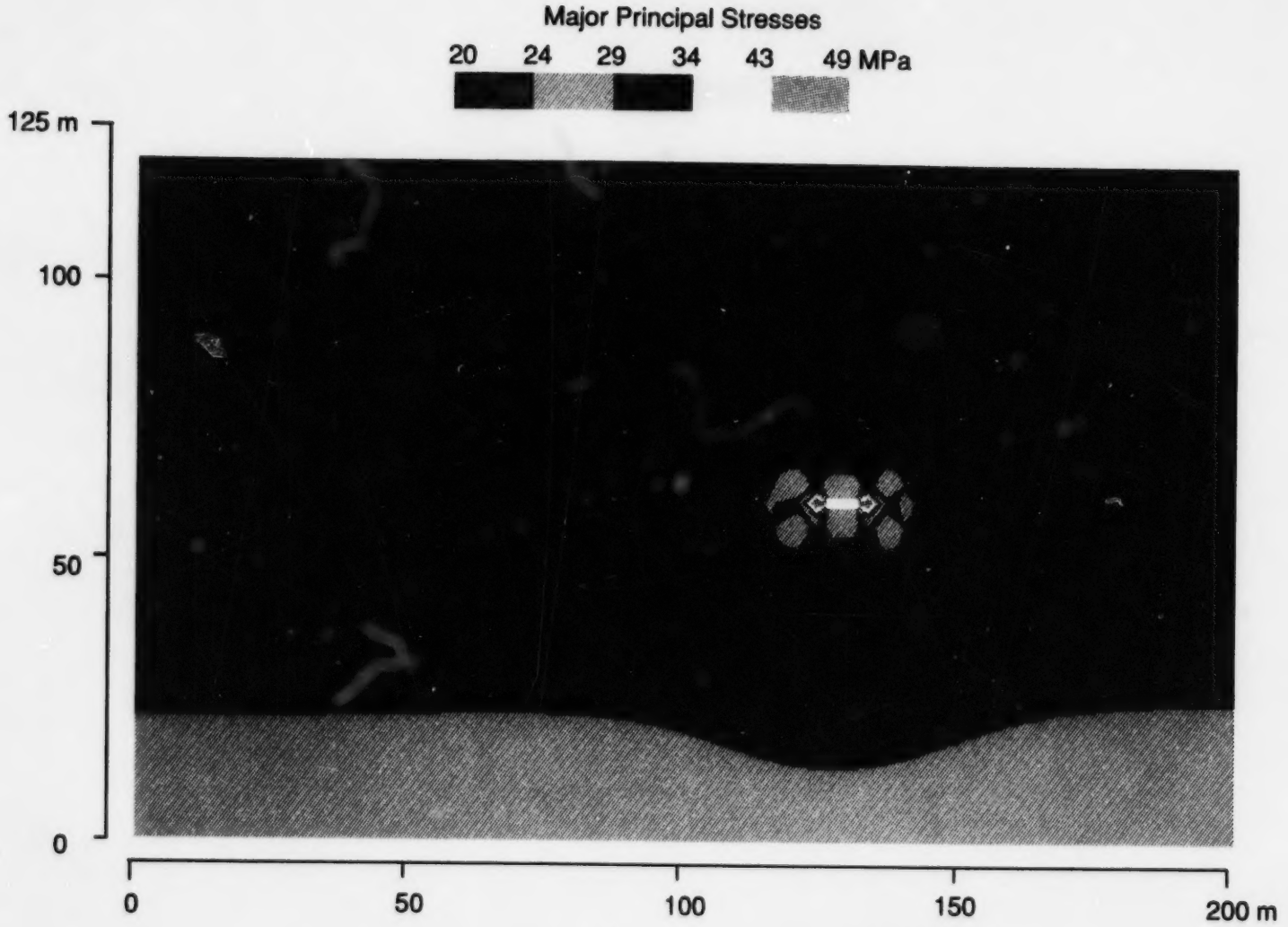

Figure 17. Major Principal Stresses at time T=0.007 days

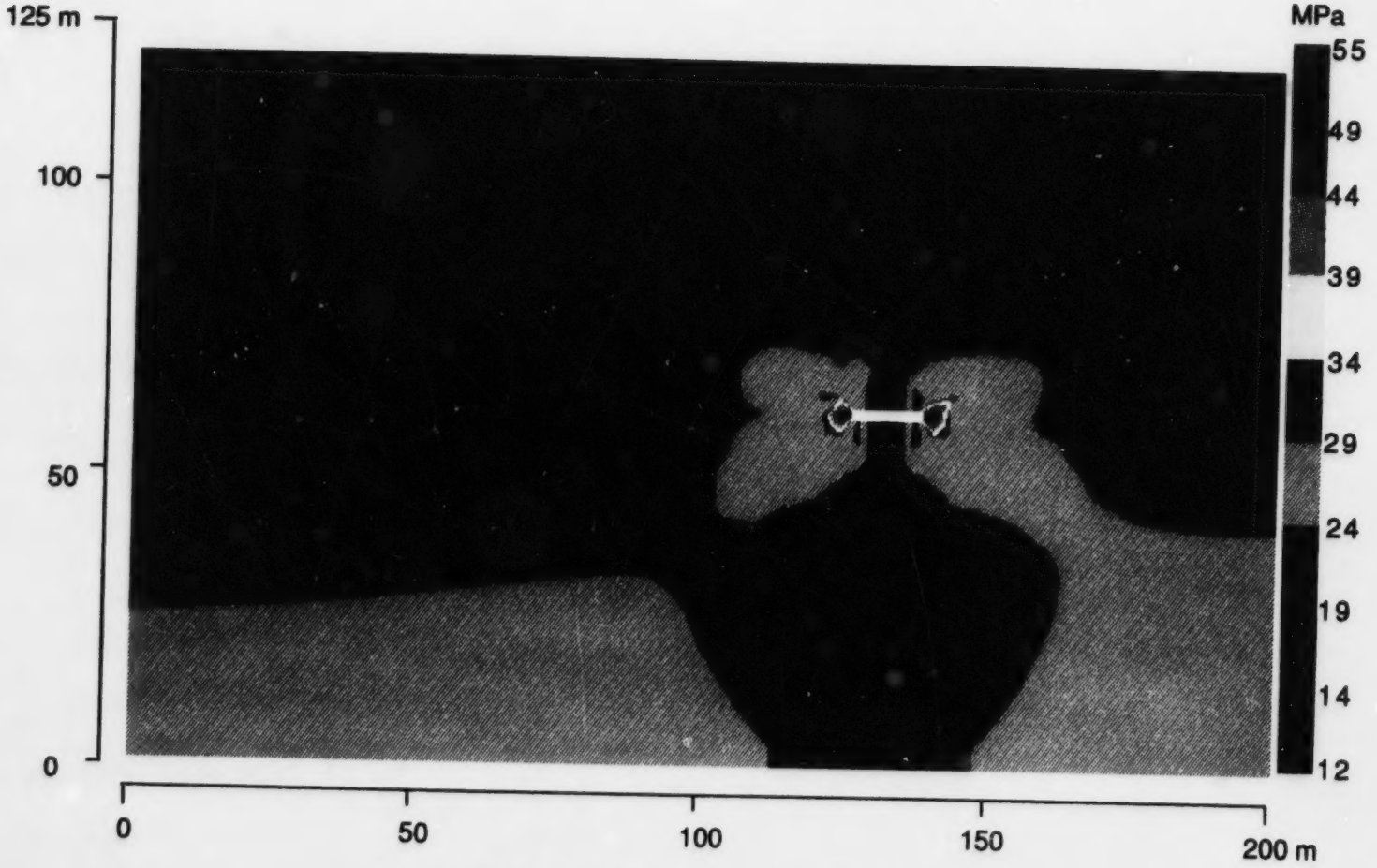

Figure 18. Major Principal Stresses at time T=14 days

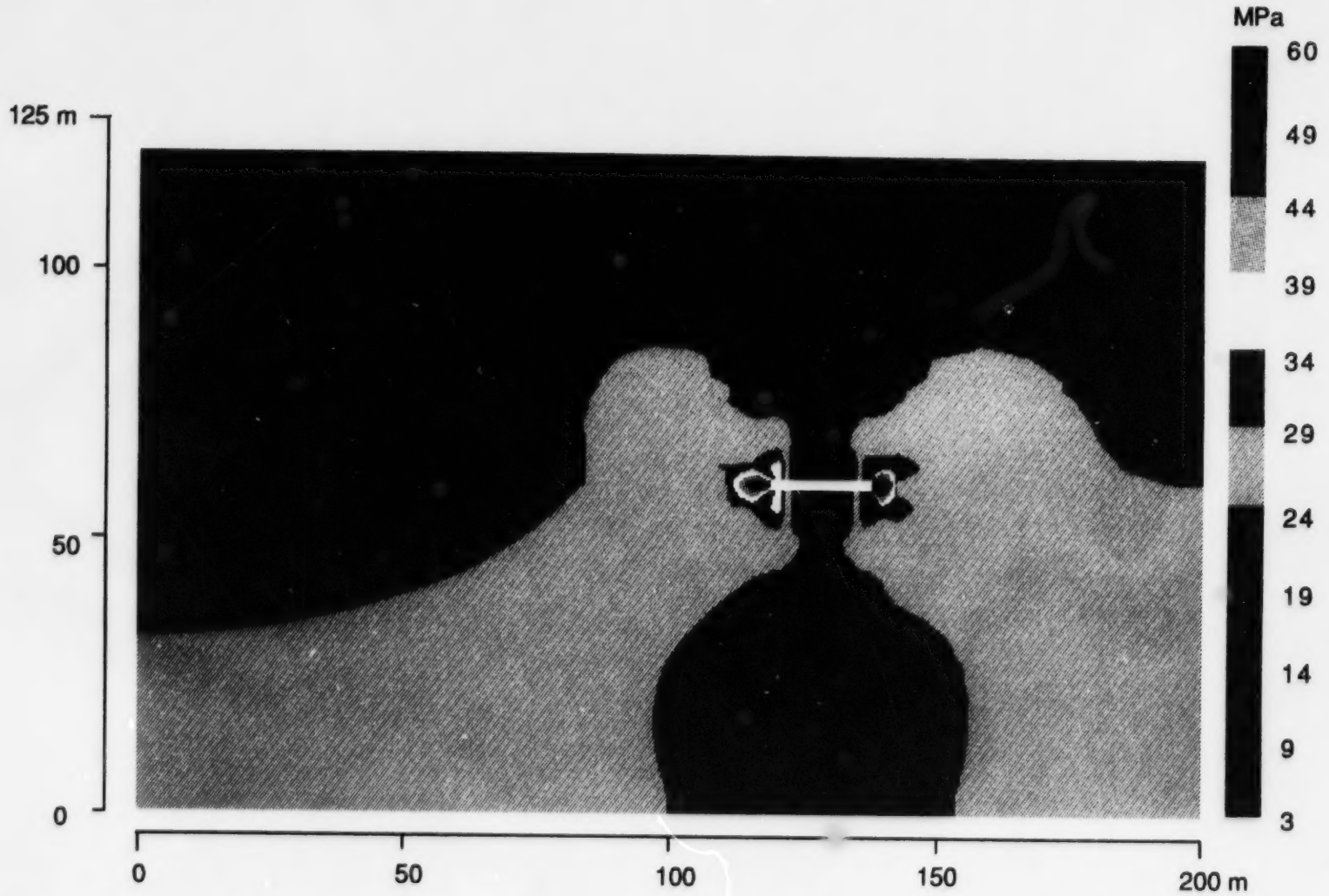

Figure 19. Major Principal Stresses at time T= 30 days

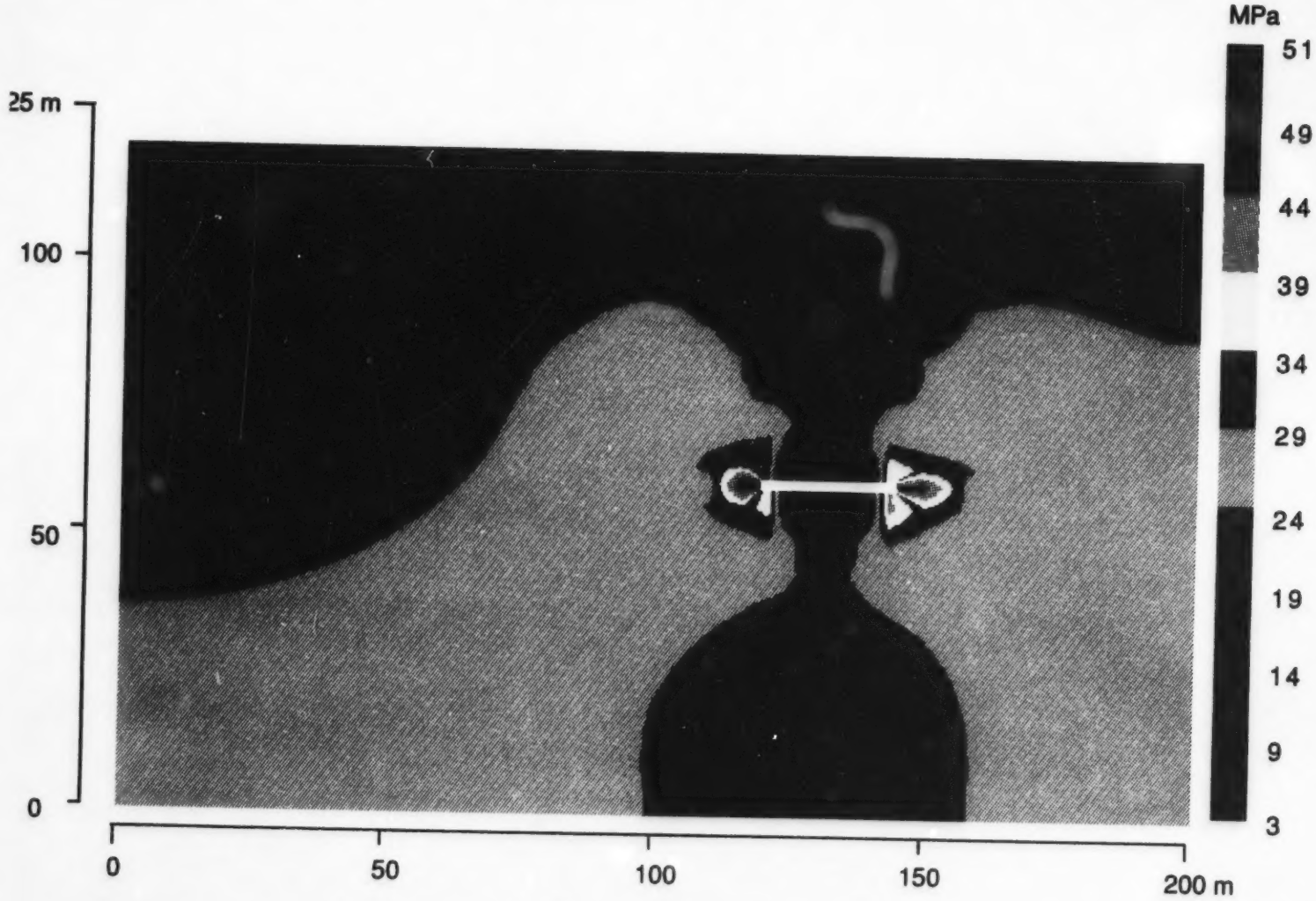

Figure 20. Major Principal Stresses at time T= 48 days

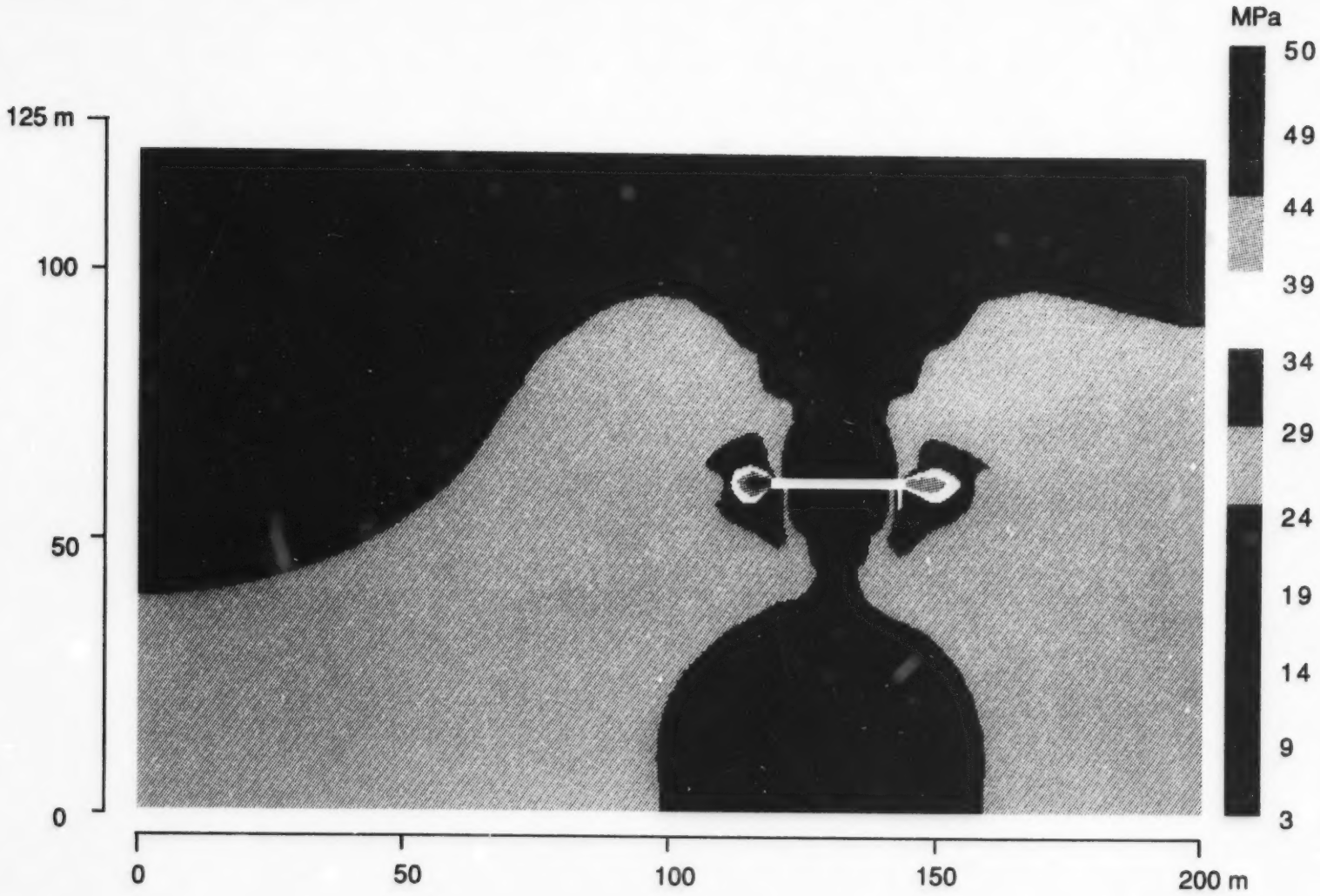

Figure 21. Major Principal Stresses at time T= 67 days

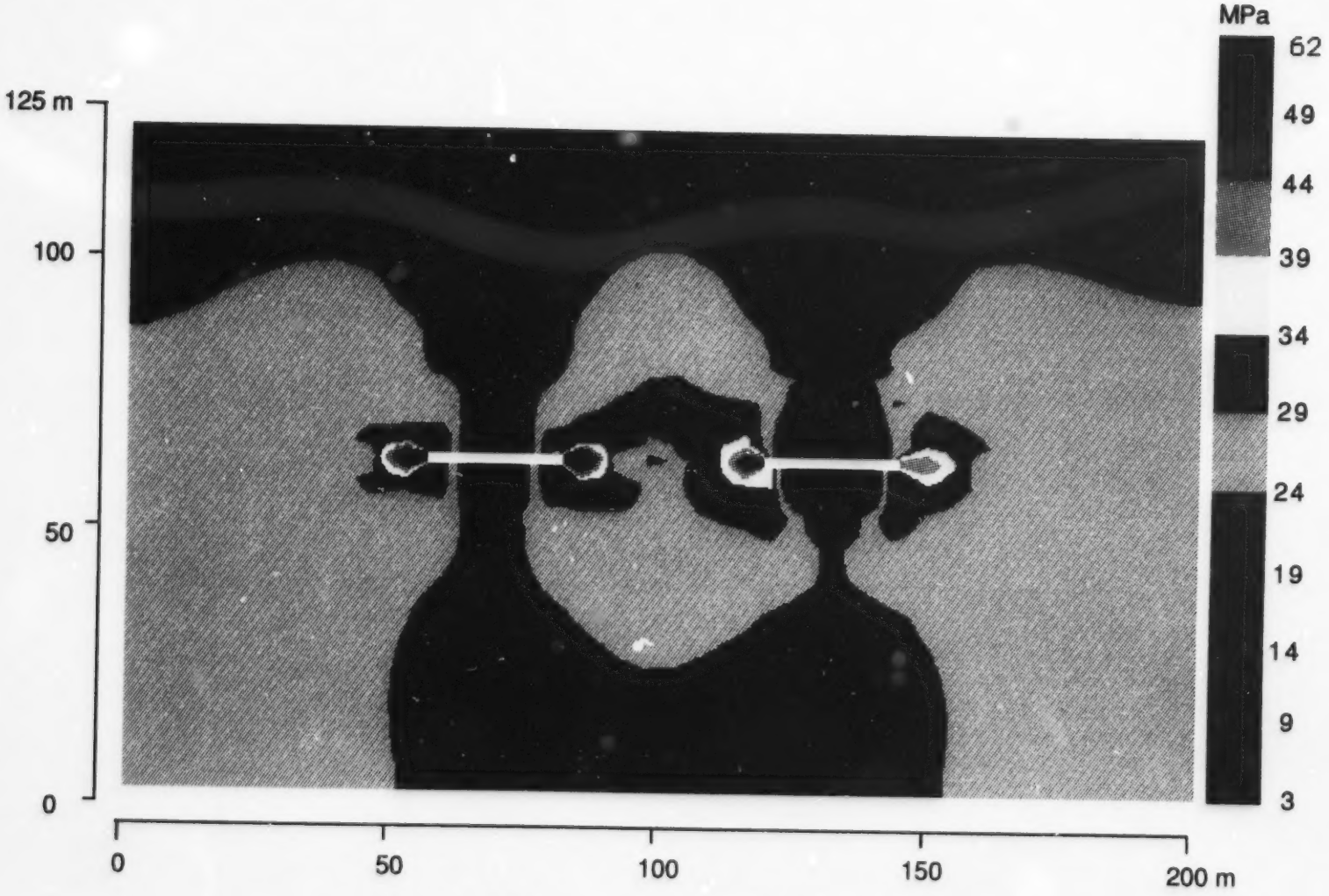

Figure 22. Major Principal Stresses at time T=129 days

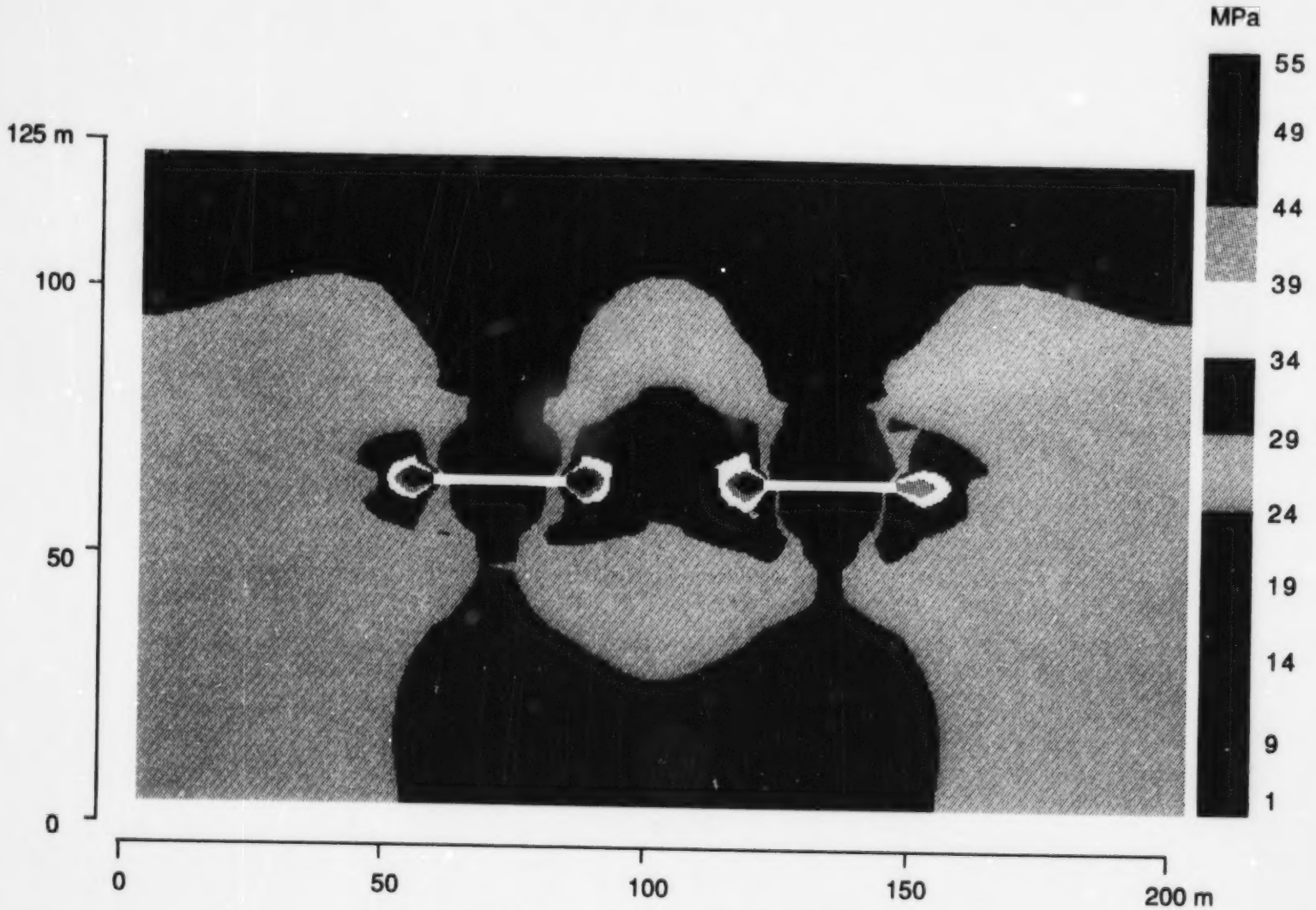

Figure 23. Major Principal Stresses at time T= 244 days

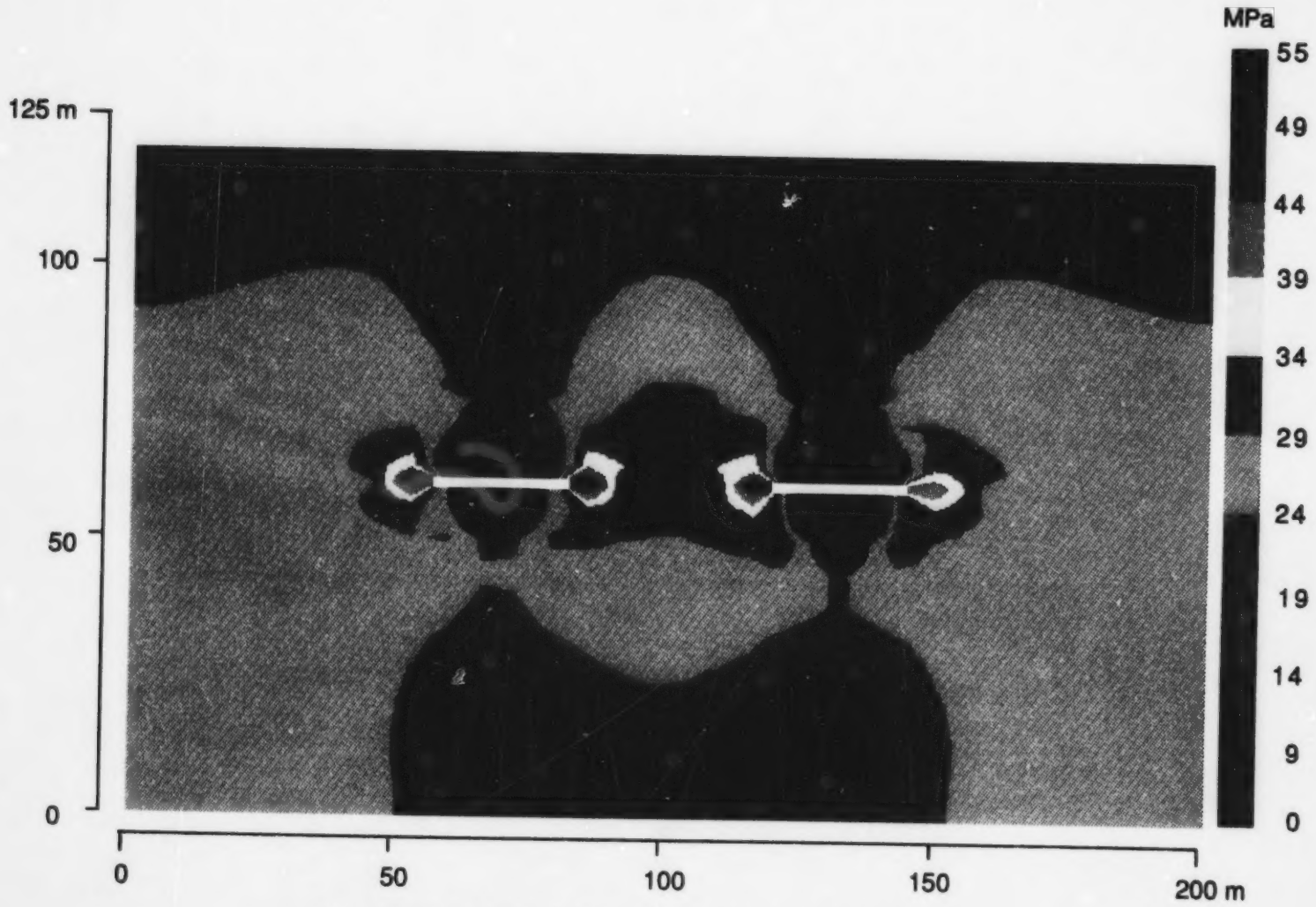

Figure 24. Major Principal Stresses at time T= 764 days

References

Carter, N.L , 1985. Creep and Creep-rupture of Rock Salt. ONWI-224, prepared by RE/SPEC Inc., Rapid City, SD, RSI-0139, Batelle Memorial Institute, Columbus, OH.

Cormeau, I., 1975. Numerical Stability in Quasistatic Elasto-visco-plasticity, Int. J. Num. Meth. Engng. vol 9, pp. 109-127.

Critescu, N., 1989. Rock Plasticity, Kluwer Academic, Dordretch, 336 p.

Mandel, J., 1971. Plasticité Classique et Viscoplasticité, Springer Verlag, Vienna.

Newmark, N.M., 1959. A method of Computation for Structural dynamics. Journal of Engng Mech. Div. Am. Soc. Civ. Engrs., vol 85, pp 67-94.

Owen, D.R.J., Hinton, E., 1980. Finite Elements in Plasticity: Theory and Practice, Pineridge Press Limited, Swansea, U.K, 394p.

Sepehr, K., Stimpson, B., 1988. Potash Mining and Seismicity: A Time Dependent Finite Element Model, International Journal of Rock Mechanics and Mining Science and Geomechanics, vol. 25, pp. 383-392.

Yu, Y.S, Ong, C.G, Mottahed, P., 1987. Computer Simulation of a Room and Pillar Mining System in a Canadian Potash Mine, Proceedings of the International Conference on Computational Plasticity held in Barcelona, Spain, Pineridge Press, Swansea, U.K.

Appendix A

Calculation of Hessian Matrix H

The hessian matrix contains partial second derivatives of the yield function F and may lead to a complicated expression depending on the complexity of F. The first derivative of the yield function with respect to stress is usually called the flow vector **a** as defined in Owen and Hinton (1980),

$$\mathbf{a} = c_1\mathbf{a}_1 + c_2\mathbf{a}_2 + c_3\mathbf{a}_3 \qquad \text{(A.1)}$$

in which constants c_1, c_2, c_3 follow the yield function used, while vectors $\mathbf{a}_1, \mathbf{a}_2, \mathbf{a}_3$ depend on stress state. Eventhough full details of the flow vector can be found in the above reference, explicit forms of c and **a** are recalled herein for matter of convenience, Table (A.1).

Table A.1 Flow Vector Constants for Different Yield Functions;

Yield criterion	c_1	c_2	c_3
Mohr-Coulomb	$\frac{1}{3}\sin\varphi$	$\{1+\tan\theta\tan 3\theta + \sin\varphi(\tan 3\theta - \tan\theta)/\sqrt{3}\}\cos\theta$	$\frac{\sqrt{3}\sin\varphi+\cos\theta\sin\varphi}{2J_2\cos 3\theta}$
Drucker-Prager	$\frac{2\sin\varphi}{\sqrt{3}(3-\sin\varphi)}$	1.0	0
Tresca	0	$2\cos\theta(1+\tan\theta\tan 3\theta)$	$\frac{\sqrt{3}\sin\theta}{J_2\cos 3\theta}$
Von Mises	0	$\sqrt{3}$	0

$$\mathbf{a}_1 = \frac{\partial I_1}{\partial \boldsymbol{\sigma}} = \{1,1,1,0,0,0\} \tag{A.2}$$

$$\mathbf{a}_2 = \frac{\partial J_2}{\partial \boldsymbol{\sigma}} = \frac{1}{2\sqrt{J_2}}\{s_{11}, s_{22}, s_{33}, 2\sigma_{23}, 2\sigma_{31}, 2\sigma_{12}\} \tag{A.3}$$

$$\mathbf{a}_3 = \frac{\partial J_3}{\partial \boldsymbol{\sigma}} = \{s_{22}s_{33} - \sigma_{23}^2 + \tfrac{J_2}{3},\ s_{11}s_{33} - \sigma_{13}^2 + \tfrac{J_2}{3},\ s_{11}s_{22} - \sigma_{12}^2 + \tfrac{J_2}{3}, \tag{A.4}$$
$$2(\sigma_{13}\sigma_{12} - s_{11}\sigma_{23}),\ 2(\sigma_{12}\sigma_{23} - s_{22}\sigma_{13}),\ 2(\sigma_{23}\sigma_{13} - s_{33}\sigma_{12})\}$$

Stress invariants J_2 and θ are defined as

$$J_2 = \frac{1}{2}\mathbf{s}:\mathbf{s}\,; \quad \mathbf{s} = \boldsymbol{\sigma} - \frac{1}{3}\mathbf{1} \otimes \text{trace}\,\boldsymbol{\sigma} \quad (\mathbf{1} = \text{Kronecker delta},\ \otimes = \text{tensor product})$$

$$\sin 3\theta = -\frac{3\sqrt{3}}{2}\frac{J_3}{J_2^{3/2}}; \quad J_3 = \det(\mathbf{s})$$

The hessian matrix is normally obtained by differentiating Eq. A.1 through the chain rule,

$$\mathbf{H} = \frac{\partial^2 F}{\partial \boldsymbol{\sigma} \otimes \partial \boldsymbol{\sigma}} = \frac{\partial \mathbf{a}}{\partial \boldsymbol{\sigma}} = c_2 \frac{\partial \mathbf{a}_2}{\partial \boldsymbol{\sigma}} + c_3 \frac{\partial \mathbf{a}_3}{\partial \boldsymbol{\sigma}} + \frac{\partial c_2}{\partial \boldsymbol{\sigma}}\mathbf{a}_2 + \frac{\partial c_3}{\partial \boldsymbol{\sigma}}\mathbf{a}_3 \tag{A.5}$$

Using the expression in Eq. (A.3), the partial derivative of $\mathbf{a}_2$ with respect to stresses can be readily calculated. Details of the derivations are not included in this appendix since they involve straightforward algebra. Only the final results are given for breveity.

Form of $\frac{\partial \mathbf{a}_2}{\partial \boldsymbol{\sigma}}$:

$$\frac{\partial \mathbf{a}_2}{\partial \boldsymbol{\sigma}} = \frac{1}{2\sqrt{J_2}}\mathbf{M}_1 - \frac{1}{4J_2^{3/2}}\mathbf{M}_2$$

where

$$\mathbf{M}_1 = \begin{bmatrix} \frac{2}{3} & -\frac{1}{3} & 0 & -\frac{1}{3} \\ -\frac{1}{3} & \frac{2}{3} & 0 & -\frac{1}{3} \\ \frac{2}{3} & 0 & 2 & 0 \\ -\frac{1}{3} & -\frac{1}{3} & 0 & \frac{2}{3} \end{bmatrix} \quad \mathbf{M}_2 = \begin{bmatrix} s_{11}^2 & s_{11}s_{22} & 2s_{11}\sigma_{12} & s_{11}s_{33} \\ s_{11}s_{22} & s_{22}^2 & 2s_{22}\sigma_{12} & s_{22}s_{33} \\ 2s_{11}\sigma_{12} & 2s_{22}\sigma_{12} & 4\sigma_{12}^2 & 2\sigma_{12}s_{33} \\ s_{11}s_{33} & s_{22}s_{33} & 2\sigma_{12}s_{33} & s_{33}^2 \end{bmatrix}. \tag{A.6}$$

Likewise, the derivative of $\mathbf{a}_3$ can be obatined from Eq. (A.4).

Form of $\frac{\partial \mathbf{a}_3}{\partial \boldsymbol{\sigma}}$:

$$\frac{\partial \mathbf{a}_3}{\partial \boldsymbol{\sigma}} = \begin{bmatrix} \frac{1}{3}(s_{11}-s_{22}-s_{33}) & \frac{2}{3}s_{33} & \frac{2}{3}\sigma_{12} & \frac{2}{3}s_{22} \\ \frac{2}{3}s_{33} & \frac{1}{3}(-s_{11}+s_{22}+s_{33}) & \frac{2}{3}\sigma_{12} & \frac{2}{3}s_{11} \\ \frac{2}{3}\sigma_{12} & \frac{2}{3}\sigma_{12} & -2s_{33} & -\frac{4}{3}\sigma_{12} \\ \frac{2}{3}s_{22} & \frac{2}{3}s_{11} & -\frac{4}{3}\sigma_{12} & \frac{1}{3}(-s_{11}-s_{22}+s_{33}) \end{bmatrix} \tag{A.7}$$

Since the constants c_2 and c_3 depend on stress invariants J_2 and θ,

$$\frac{\partial c_2}{\partial \boldsymbol{\sigma}} = \frac{\partial c_2}{\partial J_2}\frac{\partial J_2}{\partial \boldsymbol{\sigma}} + \frac{\partial c_2}{\partial \theta}\frac{\partial \theta}{\partial \boldsymbol{\sigma}}; \quad \frac{\partial c_3}{\partial \boldsymbol{\sigma}} = \frac{\partial c_3}{\partial J_2}\frac{\partial J_2}{\partial \boldsymbol{\sigma}} + \frac{\partial c_3}{\partial \theta}\frac{\partial \theta}{\partial \boldsymbol{\sigma}} \tag{A.8}$$

Stress derivatives of invariants can be readily calculated and are given by

$$\frac{\partial \theta}{\partial \boldsymbol{\sigma}} = -\frac{\sqrt{3}}{2\cos 3\theta}\left(\frac{1}{J_2^{3/2}}\mathbf{a}_3 - 3\frac{J_3}{J_2^2}\mathbf{a}_2\right) \tag{A.9}$$

$$\frac{\partial J_2}{\partial \boldsymbol{\sigma}} = \begin{cases} s_{kl} & \text{if } k = l \\ 2\sigma_{kl} & \text{if } k \neq l \end{cases} \tag{A.10}$$

Derivatives of constants c_2 and c_3, tabulated for different yield functions, are given in Tables (A.2) and (A.3).

Table A.2 Derivatives of Constants C2 for Different Yield Functions;

Yield function	$\frac{\partial c_2}{\partial J_2}$	$\frac{\partial c_2}{\partial \theta}$
Tresca	0	$2\cos\theta(\sec^2\theta\tan 3\theta + 3\tan\theta\sec^2\theta)$ $-2\sin\theta(1+\tan\theta\tan 3\theta)$
Mohr-Coulomb	0	$\cos\theta(\sec^2\theta\tan 3\theta + 3\sec^2 3\theta\tan\theta + \frac{\sin\varphi}{\sqrt{3}}(3\sec^2 3\theta - \sec^2\theta))$ $-\sin\theta(1 - \tan\theta\tan 3\theta + \frac{\sin\varphi(\tan 3\theta - \tan\theta)}{\sqrt{3}})$

Table A.3 Derivatives of Constants C3 for Different Yield Functions;

Yield function	$\frac{\partial c_3}{\partial J_2}$	$\frac{\partial c_3}{\partial \theta}$
Tresca	$-\frac{\sqrt{3}\sin\theta}{\cos 3\theta}\frac{1}{J_2^2}$	$\frac{\sqrt{3}(\cos\theta + 3\sin\theta\tan 3\theta)}{J_2\cos 3\theta}$
Mohr-Coulomb	$\frac{-\sqrt{3}(\sin\theta + \cos\theta\sin\varphi)}{2J_2^2\cos 3\theta}$	$\frac{\sqrt{3}\cos\theta - \sin\theta\sin\varphi + 3\tan 3\theta(\sqrt{3}\sin\theta + \cos\theta\sin\varphi)}{J_2\cos 3\theta}$

Appendix B

Variational Principle

Consider the following non-linear boundary value problem (BVP) stated in its strong form. Given the body force vector $\mathbf{f}=\mathbf{f}(\mathbf{x})$ and surface tractions $\mathbf{t}=\bar{\mathbf{t}}(\mathbf{x})$ where $\mathbf{x}$ is the position vector, find the displacement $\mathbf{u}=\bar{\mathbf{u}}(\mathbf{x})$ such that

$$\frac{\partial \boldsymbol{\sigma}(\mathbf{u})}{\partial \mathbf{x}} - \mathbf{f}(\mathbf{x}) = 0 \quad \text{in } \Omega \tag{B.1}$$

subject to

$$\mathbf{u} = \bar{\mathbf{u}} \quad \text{on } \Gamma_u(t); \quad \boldsymbol{\sigma}.\mathbf{n} = \bar{\mathbf{t}} \quad \text{on } \Gamma_\sigma(t) \tag{B.2}$$

where $\boldsymbol{\sigma}$ is the Cauchy stress tensor, $\bar{\mathbf{u}}$ is the prescribed displacement vector, $\bar{\mathbf{t}}$ the prescribed traction vector, $\mathbf{n}$ the normal vector to the surface and Ω is the domain of interest $\Gamma(t) = \Gamma_u \cup \Gamma_\sigma$.

It is noted that the problem domain and boundaries vary with time, and this distinguishes the present problem from a classical problem of static analysis in both linear and non-linear regimes,

$$\Omega = \Omega(t); \quad \Gamma_u = \Gamma_u(t); \quad \Gamma_\sigma = \Gamma_\sigma(t) \tag{B.3}$$

Fig. B.1 illustrates the description of motion. Applying the method of weighted residuals to (1) by multiplying by a function $\omega(t)$ and integrating over the changing domain $\Omega(t)$ result into:

$$\int_{\Omega(t)} \omega.\left(\frac{\partial \boldsymbol{\sigma}(\mathbf{u})}{\partial \mathbf{x}} - \mathbf{f}\right) d\Omega = 0. \tag{B.4}$$

It is noted that the weighting function ω should conform, with the changing domain Ω at time t. When integrating Eq. (B.4) by parts and noting Eq. (B.2), one finally gets,

$$W_{\text{int}}(t) = W_{\text{ext}}(t), \tag{B.5}$$

where

$$W_{\text{int}}(t) = \int_{\Omega(t)} \omega \boldsymbol{\sigma}\, d\Omega, \tag{B.6}$$

and

$$W_{ext}(t) = \int_{\Omega(t)} \omega.\mathbf{f}\, d\Omega + \int_{\Gamma_\sigma(t)} \omega.\bar{\mathbf{t}}\, d\Gamma. \tag{B.7}$$

Equation (B.5) basically states the classical principle of virtual work, with the difference that now one is faced with a time varying domain and boundary problem.

Within the framework of finite elements, global force equilibrium must be achieved by assuming the change in domain and boundary to be represented by a constant piecewise function in the time domain. In physical terms, this is equivalent to modelling placement of filling or excavation as instantaneous events which can be modelled discretely by addition or substraction of nodes and elements from the original finite element mesh.

In a finite element context, the time interval of interest is discretized in incremental time steps according to

$$[0,T] = \bigcup_{n=1}^{N} [t_n, t_{n+1}]. \tag{B.8}$$

Within a typical time step, discrete equilibrium must be satisfied, i.e.

$$(\mathbf{F}_{\text{int}})_{n+1} - (\mathbf{F}_{\text{ext}})_{n+1} = 0, \tag{B.9}$$

in which

$$(\mathbf{F}_{\text{int}})_{n+1} = \mathbf{F}_{\text{int}}(\mathbf{u}_{n+1}) = \bigcup_{e=1}^{nel} \mathbf{f}^e_{\text{int}}(\boldsymbol{\sigma}_{n+1}). \tag{B.10}$$

Here $\bigcup$ denotes the assembly operator over active elements. Similarly,

$$(\mathbf{F}_{\text{ext}})_{n+1} = \bigcup_{e=1}^{nel} \mathbf{f}^e_{\text{ext}}, \tag{B.11}$$

where

$$\mathbf{f}^e_{\text{int}} = \int_{\Omega_{n+1}} \mathbf{B}^T_{n+1} : \boldsymbol{\sigma}_{n+1}\, d\Omega, \tag{B.12}$$

and the external force vector is represented by

$$\mathbf{f}^{e}_{\text{ext}} = \int_{\Omega_{n+1}} \mathbf{N}^{T}_{n+1} : \mathbf{f}\, d\Omega + \int_{\Gamma_{n+1}} \mathbf{N}^{T}_{n+1} : \bar{\mathbf{t}}\, d\Gamma. \tag{B.13}$$

During the time interval $[t_n, t_{n+1}]$, the stress rate

$$\dot{\boldsymbol{\sigma}} = \mathbf{C}^{E} : (\dot{\boldsymbol{\varepsilon}} - \dot{\boldsymbol{\varepsilon}}^{vp}) \tag{B.14}$$

may be integrated to obtain

$$\boldsymbol{\sigma}_{n+1} = \boldsymbol{\sigma}_n + \mathbf{C}^{E} : \Delta\boldsymbol{\varepsilon}_n - \mathbf{C}^{E} : [(1-\alpha)\dot{\boldsymbol{\varepsilon}}^{vp}_n + \alpha\dot{\boldsymbol{\varepsilon}}^{vp}_{n+1}]\Delta t_n. \tag{B.15}$$

Since

$$\dot{\boldsymbol{\varepsilon}}^{vp}_{n+1} = \dot{\boldsymbol{\varepsilon}}^{vp}_n + \Delta\dot{\boldsymbol{\varepsilon}}^{vp}_n, \tag{B.16}$$

with the change in viscoplastic strain rate obtained by differentiating the flow rule,

$$\begin{aligned} \Delta\dot{\boldsymbol{\varepsilon}}^{vp}_{n+1} &= \mathbf{H}_n : \Delta\boldsymbol{\sigma}_n, \\ \mathbf{H}_n &= \Gamma[< \Phi(F) > \frac{\partial^2 F}{\partial\boldsymbol{\sigma} \otimes \partial\boldsymbol{\sigma}} + \frac{\partial < \Phi >}{\partial\boldsymbol{\sigma}} : \frac{\partial F}{\partial\boldsymbol{\sigma}}]. \end{aligned} \tag{B.17}$$

The new stress at time t_{n+1} becomes,

$$\boldsymbol{\sigma}_{n+1} = \boldsymbol{\sigma}_n + \mathbf{C}^{E} : \Delta\boldsymbol{\varepsilon}_n - \Delta t_n \mathbf{C}^{E} : [\dot{\boldsymbol{\varepsilon}}^{vp}_n + \alpha\mathbf{H}_n : \Delta\boldsymbol{\sigma}_n]. \tag{B.18}$$

Further re-arrangement of the above leads to an explicit expression for the stress change, i.e.

$$\Delta\boldsymbol{\sigma}_n = \mathbf{D}^{T}_n : [\Delta\dot{\boldsymbol{\varepsilon}}_n - \Delta t_n \dot{\boldsymbol{\varepsilon}}^{vp}_n], \tag{B.19}$$

$$\mathbf{D}^{T}_n = [\mathbf{C}^{E^{-1}} + \alpha\Delta t_n \mathbf{H}_n]^{-1}. \tag{B.20}$$

The stress change can be replaced into the equation of equilibrium (B.9). Noting Eqs. (B.12) and (B.13), one gets:

$$\bigcup_{e=1}^{nel}\int_{\Omega_{n+1}} \mathbf{B}_{n+1}^T:\mathbf{D}_n^T:\mathbf{B}_{n+1}d\Omega\,\Delta\mathbf{u}_n = \bigcup_{e=1}^{nel}\left\{\int_{\Omega_{n+1}} \mathbf{N}_{n+1}^T:\mathbf{f}\,d\Omega + \int_{\Gamma_{n+1}} \mathbf{N}_{n+1}^T:\bar{\mathbf{t}}\,d\Gamma - \int_{\Omega_{n+1}} \mathbf{B}_{n+1}^T:\boldsymbol{\sigma}_n d\Omega\right\}$$
$$+\bigcup_{e=1}^{nel}\Delta t_n\int_{\Omega_{n+1}} \mathbf{B}_{n+1}^T:\mathbf{D}_n^T:\dot{\boldsymbol{\varepsilon}}_n^{vp}\,d\Omega. \tag{B.21}$$

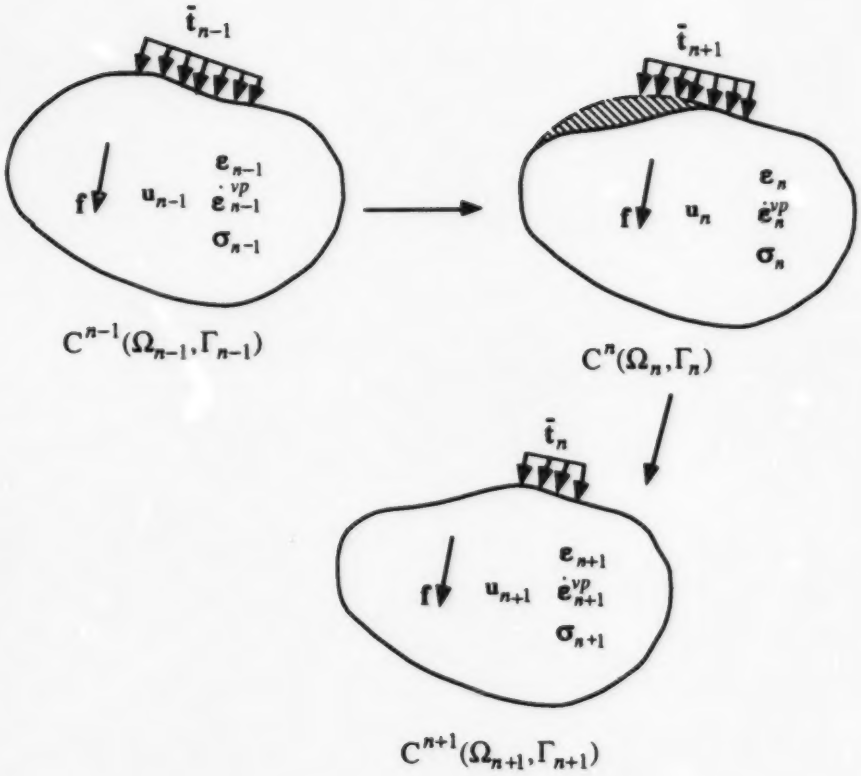

Figure B.1 Description of motion for excavation/fill;